HURRICANE HILDA, 1964

II. STRUCTURE AND BUDGETS OF THE HURRICANE ON OCTOBER 1, 1964

HARRY F. HAWKINS and DARYL T. RUBSAM

National Hurricane Research Laboratory, Research Laboratories, ESSA, Miami, Fla.

ABSTRACT

Aircraft data from five levels (900 to 180 mb.) are used to depict the structure of a mature hurricane. Horizontal analyses, vertical cross sections, and various budgets, which have been prepared from the research flight data only, are presented. New estimates of the drag coefficient under hurricane conditions are derived from a different formulation utilizing the momentum budget in the inflow layer.

1. INTRODUCTION

On Oct. 1, 1964, as hurricane Hilda was still deepening and already an intense hurricane [6], the Research Flight Facility in support of the National Hurricane Research Laboratory launched a special data-gathering effort. The plan was to gather meteorological data throughout the intense core of the storm at five levels. Each of the two DC-6's was responsible for data sampling at two levels at or below 500 mb. The first DC-6 took observations along the flight pattern shown in figure 1a at 900 mb. (3,240 ft. PA). When this pattern was completed, the plane climbed to 750 mb. (8,090 ft. PA) and executed a pattern similar to that shown in figure 1b. The other DC-6 flew a pattern similar to that in figure 1a at 650 mb. (11,780 ft. PA), then climbed to 500 mb. (18,280 ft. PA), and followed the pattern shown in figure 1b. The high altitude jet at 180 mb. (40,870 ft. PA) flew the pattern shown in figure 1c and then had to head for its staging base because of its extremely short range. This five-level collection of data is unique in the NHRL-RFF files. It presented the best vertical resolution that had become available up to that date, and for this and other reasons it seemed appropriate that the data should be analyzed exhaustively and that budget studies for various parameters be prepared where the data permitted.

2. DATA COMPOSITING AND DATA LIMITATIONS

The primary tool used in compositing the data about the moving storm is the time-lapse radar film record. At frequent intervals, when the radar eye of the storm is discernible on the film, the relative range and bearing of the plane to the geometric center of the radar eye wall is tabulated. These relative fixes of the plane to the storm are fed into the computer, which interpolates between fixes using the known motion of the storm and the Doppler navigation information of the motion of the plane (carried on the magnetic tape together with the meteorological observations). For some purposes, this compositing technique and its accuracy are quite satisfactory. For other purposes, the present equipment permits only marginally acceptable compositing. For instance, if the plane is located 60 n.mi. from the eye center and is misplaced azimuthally by a distance of 1 n.mi., i.e., 1°, then an error in the radial wind component equal to sin 1° multiplied by the wind speed will result. Thus, if the wind speed is 60 kt., the error in radial wind speed will be 1 kt. Most meteorological parameters have very small tangential or azimuthal gradients, however, and such errors may be quite unimportant for many of the uses that may be made of these data.

The winds were Doppler winds, which are measured relative to the surface over which the plane is flying. If the surface interrogated by the radar beam has a mean motion in a given direction, the wind computed by the Doppler system will be in error by an amount equal and opposite to the motion of the reference plane. Most of the wind speeds with which we are concerned are large, while most estimates of the net water motion (particularly the radial motion) are quite small. O'Brien and Reid [17] used a numerical model in arriving at an estimate of the maximum radial water motion of around 1 kt. and a maximum tangential motion of 2 to 3 kt. These velocities, however, were means for the water motion over depths of the order of 60 m. In the present study all winds were calibrated (post-flight) for errors in true air speed and drift.

Temperatures were measured by vortex thermometers requiring no dynamic correction. Many researchers who have used vortex temperatures are of the opinion that during flights through cloud and falling rain, particularly heavy rain, the values obtained may be too low by as much as 1.5°C. to 2.0°C. Having examined the data, we found no satisfactory systematic manner in which to apply this knowledge. In some situations, use of such corrections apparently improved the thermal structure, but in others where the correction apparently should also be applied, it made the thermal structure less acceptable.

315-521 O - 68 - 5

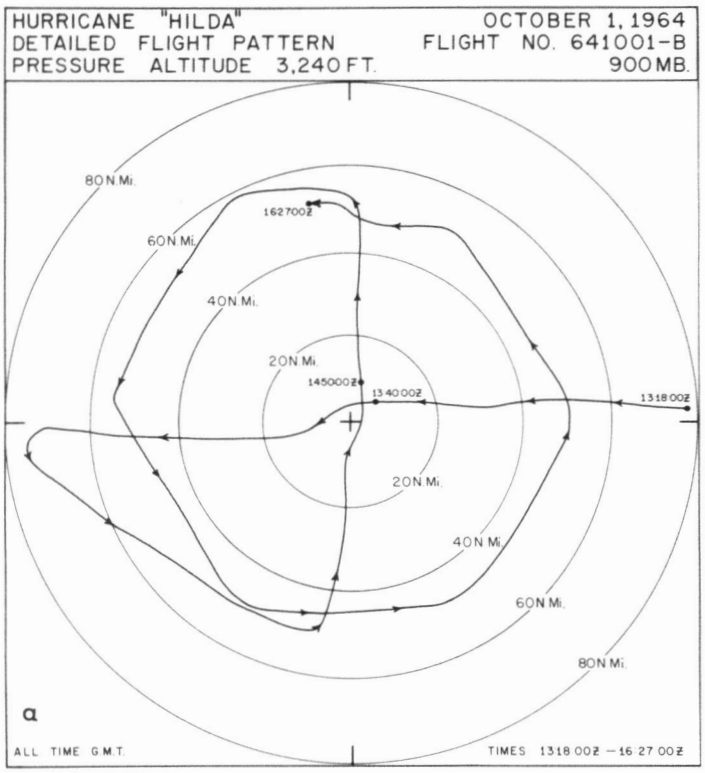

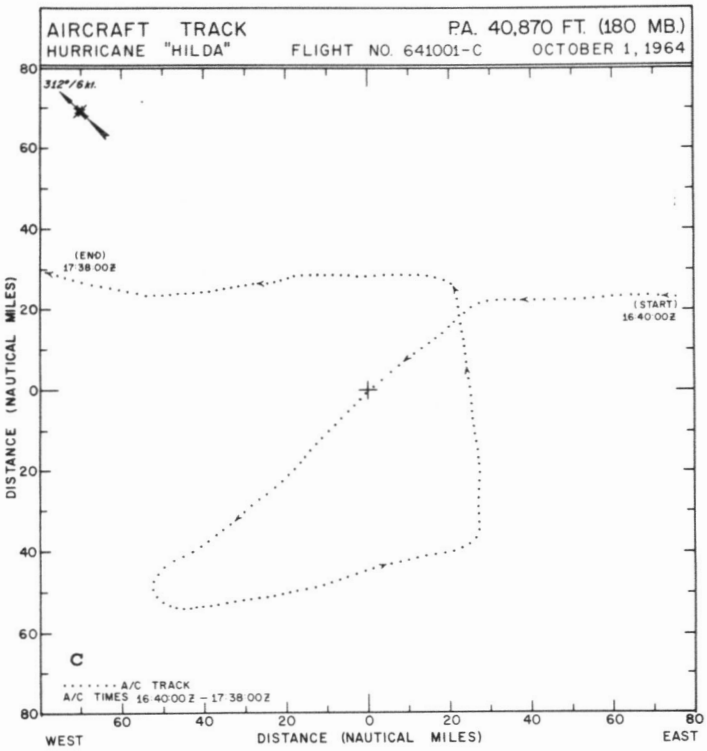

FIGURE 1.—Flight pattern, relative to the moving hurricane center (at 0 n.mi. radius), at (a) low level, (b) 500 mb., and (c) 180 mb.

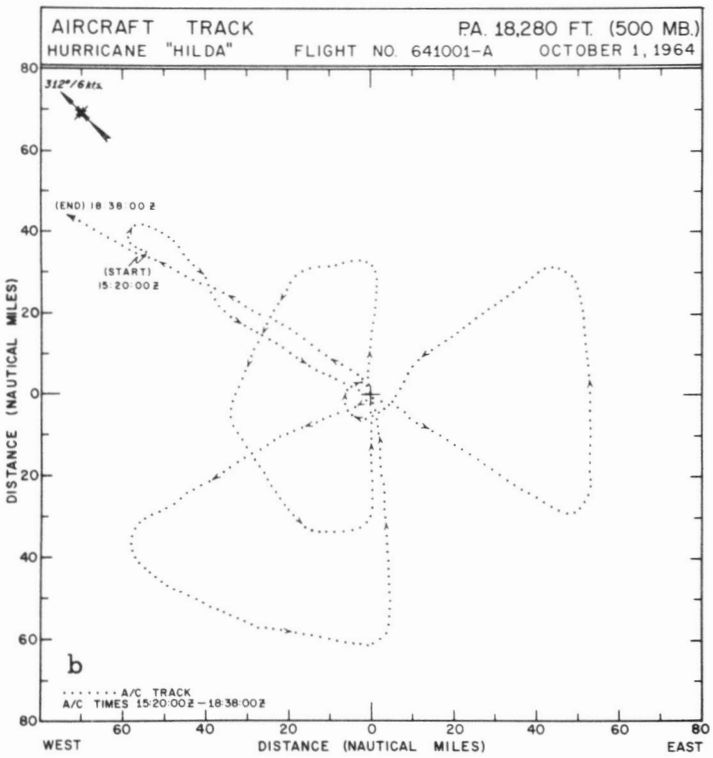

Consequently, the temperatures were not corrected for "in" or "out" of falling rain, nor were any systematic corrections deemed applicable to the DC-6 vortex thermometer readings as a result of the temperature checks made with the radiosonde runs at Key West and Miami. The high altitude aircraft temperatures were finally judged to be 3°C. too high after extensive checking of other flights that season, and consistency tests of the data and the soundings on the day of the flight.

3. HORIZONTAL ANALYSES

The data coverage made detailed horizontal analyses possible out to a radial distance of 70 to 80 n.mi. In the interests of brevity, and because intermediate changes were relatively small, we present the analyses at only three levels: 900 mb., 500 mb., and 180 mb.

The streamline analyses for these levels are presented in figure 2. Figure 2a shows that the air motion relative to the moving storm at 900 mb. was a nearly circular, fairly symmetric, spiral indraft. Similar flows with progressively decreasing indrafts were analyzed at the 750- and 650-mb. levels. At 500 mb. (fig. 2b) the inner 40 n.mi. showed little indraft or outdraft although at greater radii a slight outdraft was evident. Hence the "low level" inflow layer terminated somewhere between the 650- and 500-mb. levels. At 180 mb. (fig. 2c) the inner cyclonic circulation was preserved. Strong diffluence, beginning some 25 to 30 n.mi. out, was observed mainly east and southeast of the storm center. To the northwest and to the southeast, the wind turned anticyclonically.

Maximum wind speeds (relative to the moving center) were recorded between 100 and 110 kt. at both the 900-mb. (fig. 3a) and 750-mb. levels, where the radius of maximum

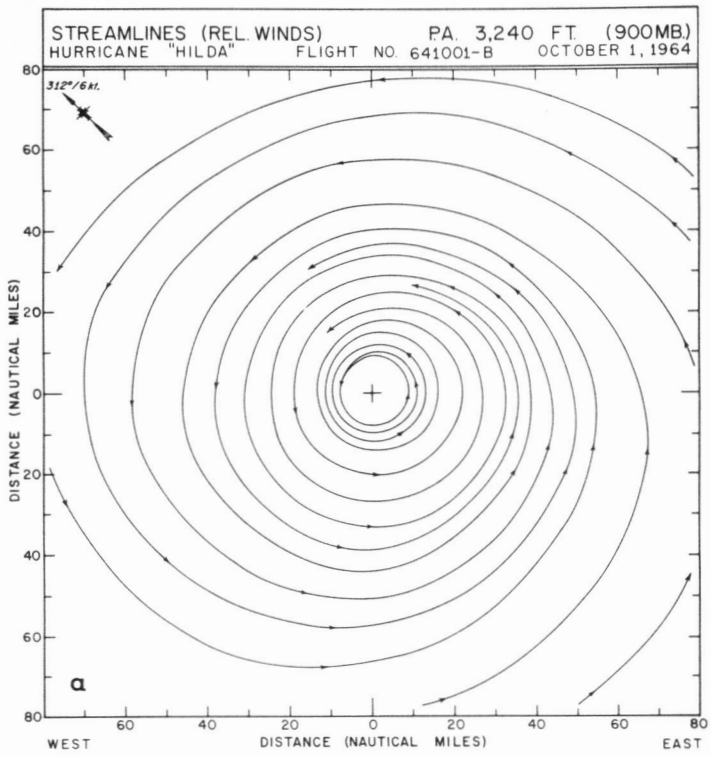

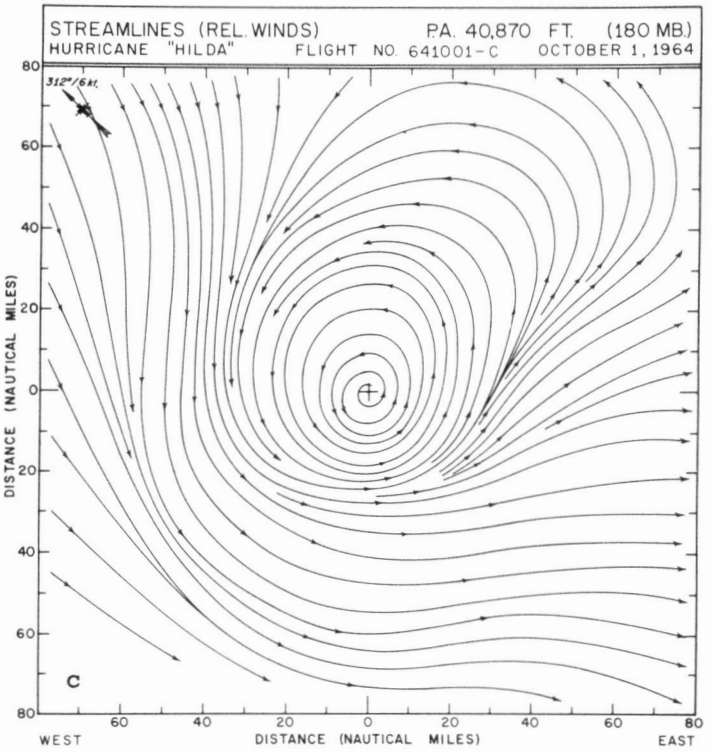

FIGURE 2.—Streamline pattern at (a) low level, showing the nature of the spiral inflow relative to the moving center; (b) 500 mb., showing practically no significant inflow or outflow; (c) 180 mb., showing outflow from the storm and strong diffluence to the southeast.

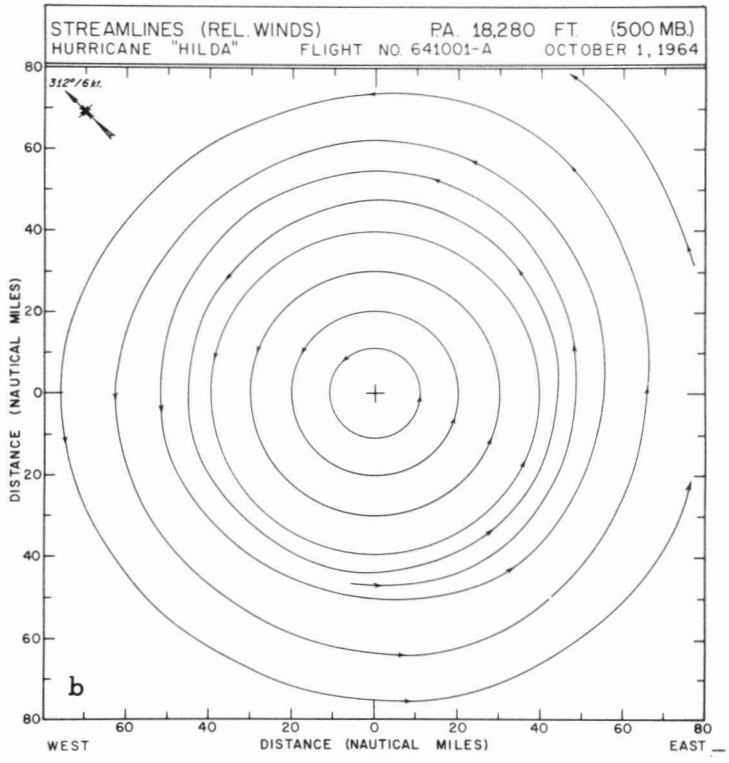

winds was about 12 n.mi. Note that these two levels were investigated by the same aircraft so that there was an effective time difference of about 3 hr. between the data samples. At 900 mb. the isotach analysis showed a relatively simple pattern with fairly strong radial gradients but weak tangential gradients. The pattern appeared to become more complex with elevation at least to around 500 mb. (fig. 3b), where numerous small centers of maximum and minimum wind speed appeared. The 180-mb. wind speeds (fig. 3c) were surprisingly well sustained with height. Some 18 n.mi. from the center 50-kt. winds were associated with the cyclonic core of the hurricane. Some 30 n.mi. southwest from the center, another, larger wind speed maximum of 50 kt. appeared to be more closely related to the larger scale circulation in which the vortex was embedded.

Even at the low level of 900 mb. the warm-core structure of hurricane Hilda was manifest (fig. 4a). Temperatures in the eye reached 23°C. at this level. Some 40 to 50 n.mi. out, on the other hand, temperatures averaged between 18 and 19°C. It is not impossible that this fairly strong temperature difference was enhanced because of the vortex thermometer deficiency previously discussed. At 500 mb. (fig. 4b) the strongest gradients were in or near the eye wall. Temperatures were above 3.0°C. in the center of the eye and decreased sharply with distance just outside the eye. This first annulus of cool air outside the eye was succeeded by warmer air at greater radii until a second cool pool was met some 70 n.mi. to southwest of the center. All in all the 500-mb. temperature pattern seemed more

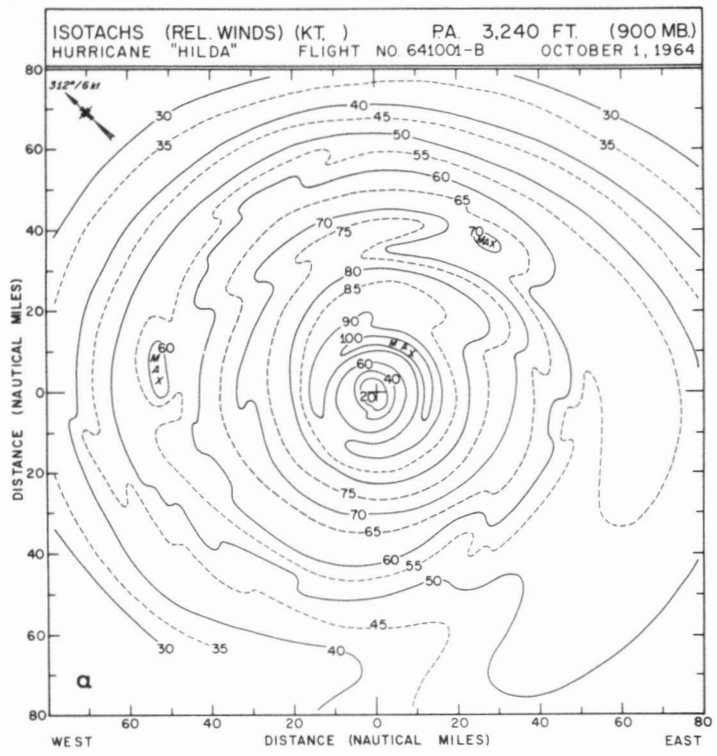

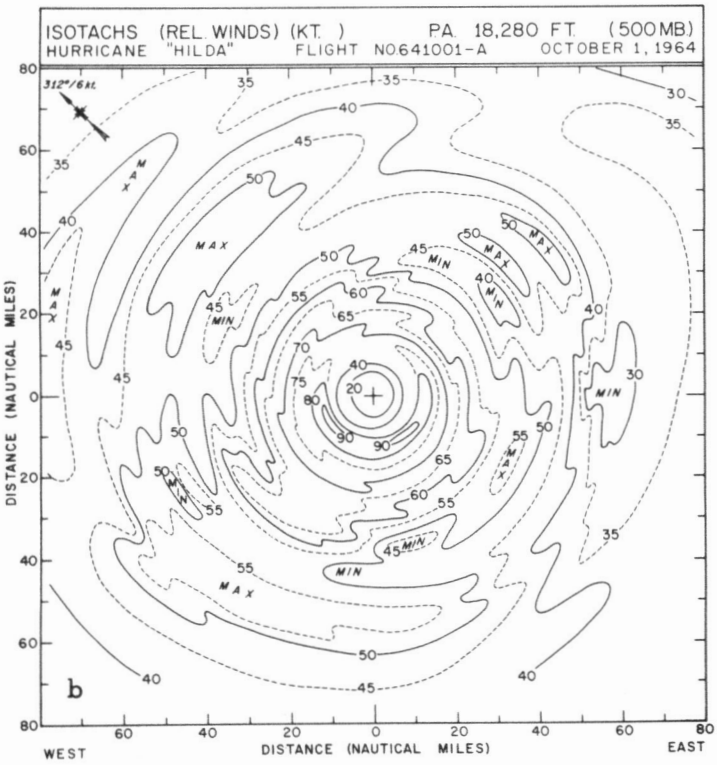

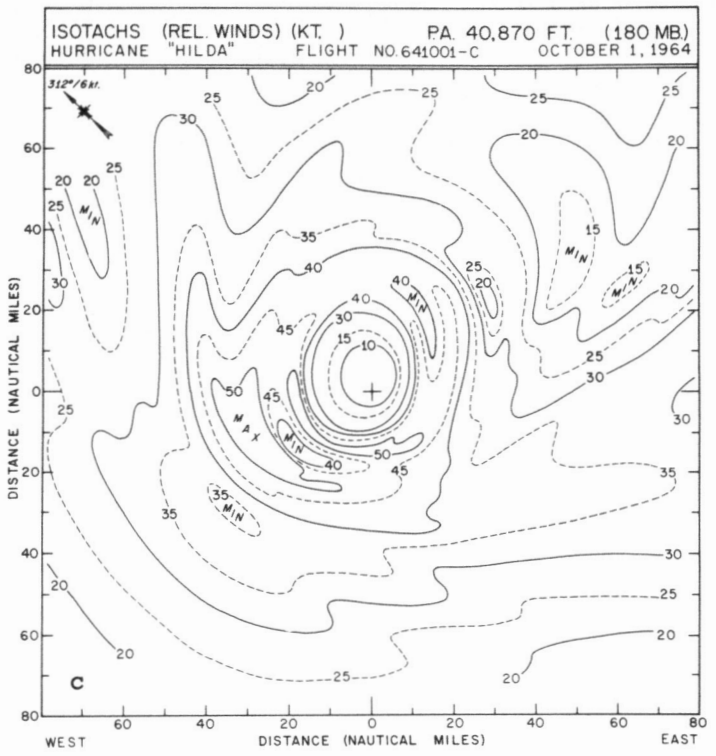

FIGURE 3.—Isotachs at (a) 900 mb.; (b) 500 mb. (Note the increase in complexity of the pattern, presumably a reflection of the turbulent structure of the storm.); and (c) 180 mb.

complex than one might have anticipated *a priori*. At 180 mb. (fig. 4c) the pattern was mainly one of circular symmetry about the eye with temperatures rising (as the eye was approached) to the highest value (−48°C.), which was encountered in the eye.

The 900-mb. *D*-values presented in figure 5a show a structure of nearly concentric circles. Figure 5b shows a very similar structure for 500 mb., except for reduced gradients. There were usable *D*-values from the jet aircraft at 180 mb. and these were merged with values computed hydrostatically using figure 5b as a base and employing the temperature data from 500 and 180 mb. and the humidity data from 500 mb. Figure 5c shows the further weakening of the cyclonic vortex with height that one would expect in a warm-core vortex.

The final horizontal analyses are for the specific humidities for 900 and 500 mb., shown in figures 6a and b respectively. No humidity measurements were taken from the jet aircraft. For the most part specific humidities increased with decreasing radius until the eye was reached. In the eye, they remained at or near the maximum. At first glance their high values may seem somewhat surprising but, as pointed out by LaSeur and Hawkins [12], the temperatures rise so rapidly as the eye is approached that within the eye the relative humidities are less than they are in the surrounding wall cloud and in the adjacent regions beyond.

4. VERTICAL CROSS SECTIONS

The similarities in the patterns flown by the various planes were designed for specific purposes. The first traverses (see fig. 7) were planned from northeast to southwest through the storm center, but because the

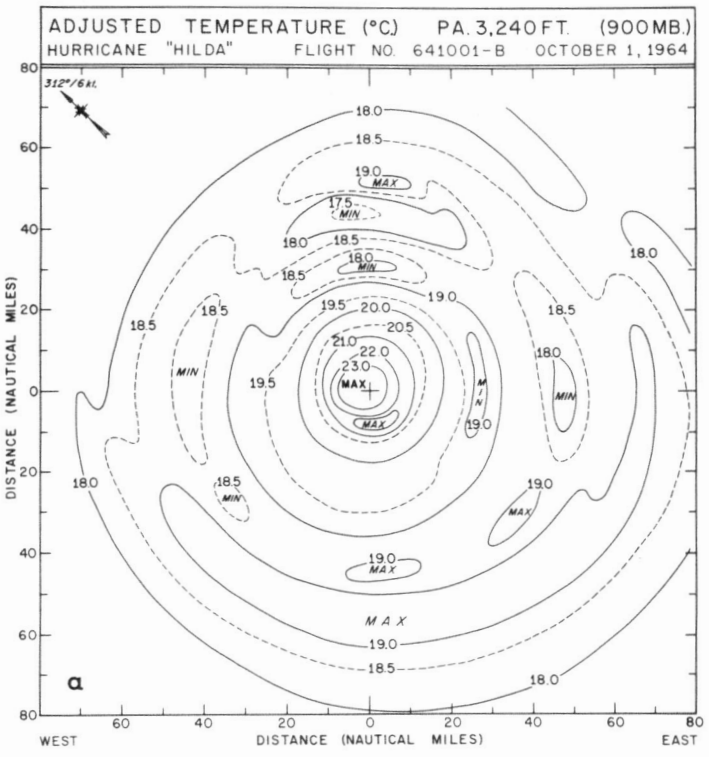

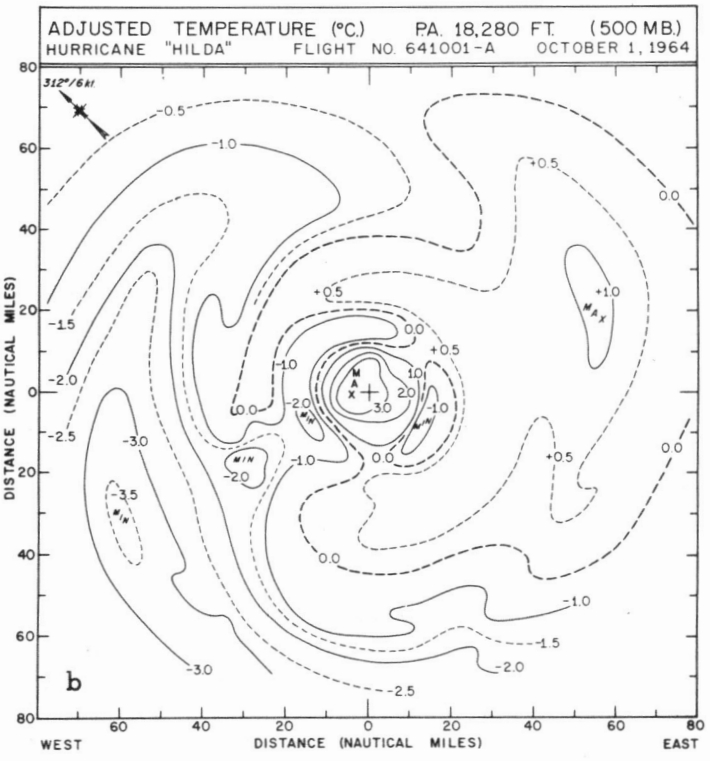

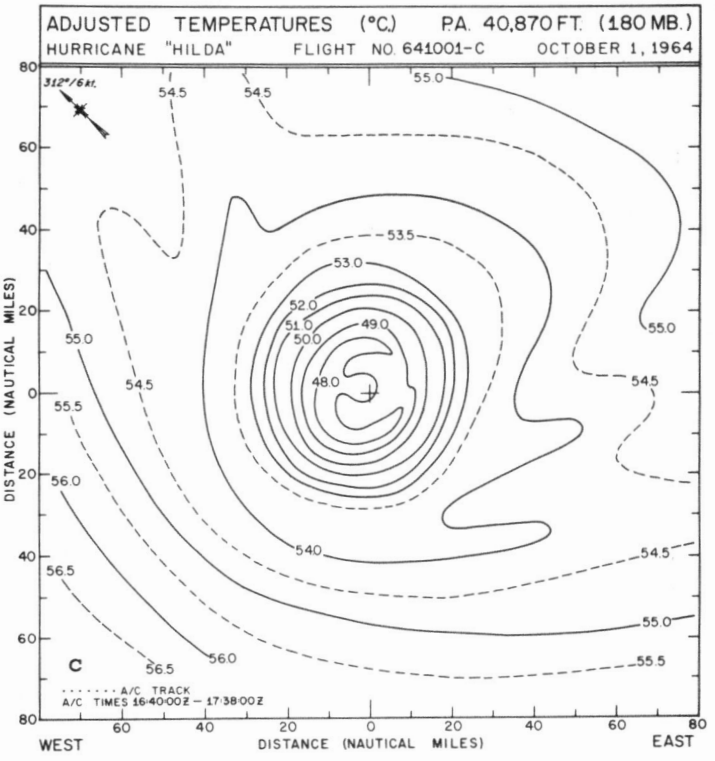

FIGURE 4.—Temperature at (a) 900 mb., showing a marked tendency towards a warm-core structure; (b) 500 mb., showing a total temperature rise only slightly larger than at 900 mb.; and (c) 180 mb., showing a smooth, relatively simple temperature pattern. All temperatures are negative in c.

storm was a little farther north than anticipated, the first penetration ran more from east-northeast to west-southwest at 900 and 650 mb. These planes were subsequently joined by the jet for a three-plane traverse at 750, 500, and 180 mb. The total time spread was about 5 hr. Rather than being "stacked" vertically the planes had tangential separations ranging up to around 40 mi. The data were composited, however, as if synoptic in time and superposed in space for the purpose of constructing vertical cross sections. When necessary, the data were subjectively smoothed and reasonable allowances were made for the method of compositing.

TEMPERATURES

Based on the data from the five levels (800, 750, 650, 500, and 180 mb.) soundings were constructed at 10-n.mi. intervals on either side of the storm out to 60 n.mi. on the east and 70 n.mi. on the west side (fig. 8). The lowest portions of the soundings, i.e., below 900 mb., were constructed under the assumptions that: 1) the cloud ceiling lowered from 1,500 ft. at 70 n.mi. to 800 ft. at the eye wall, which seemed reasonable in the light of our experience in low level hurricane penetrations; 2) the sounding was saturated, or very nearly so, from the 900-mb. observation down to the lifting condensation level at the cloud base; and 3) from cloud base to ocean surface the sounding was essentially dry adiabatic. The terminal sea level pressures were estimated from calculations that extrapolated the 900-mb. D-values to equivalent sea level pressures and from preliminary analysis of the D-value profile (to be discussed later). For the most

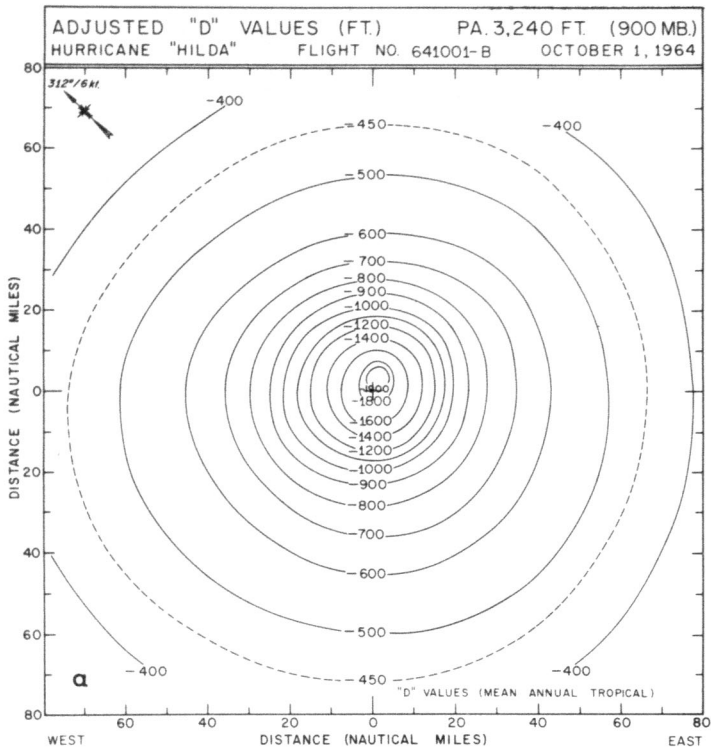

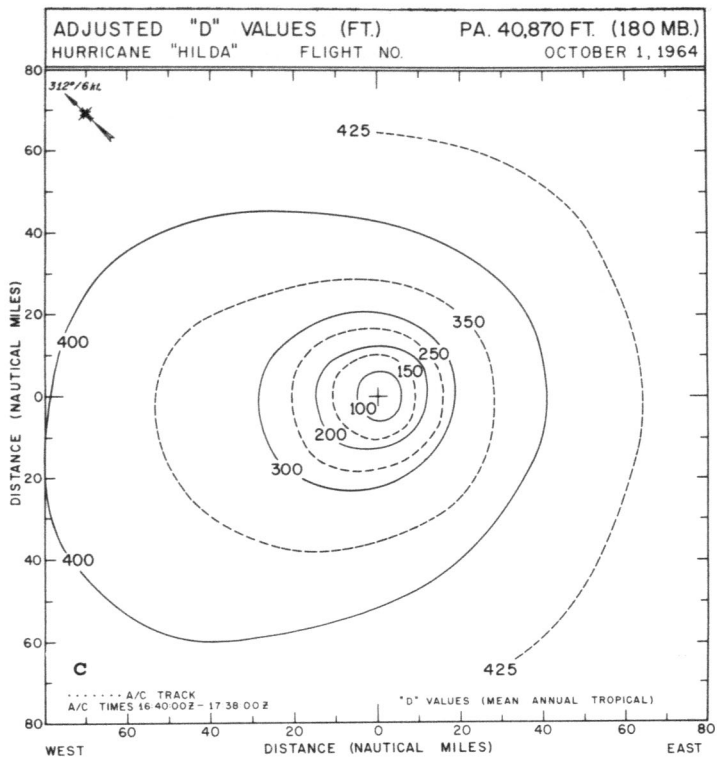

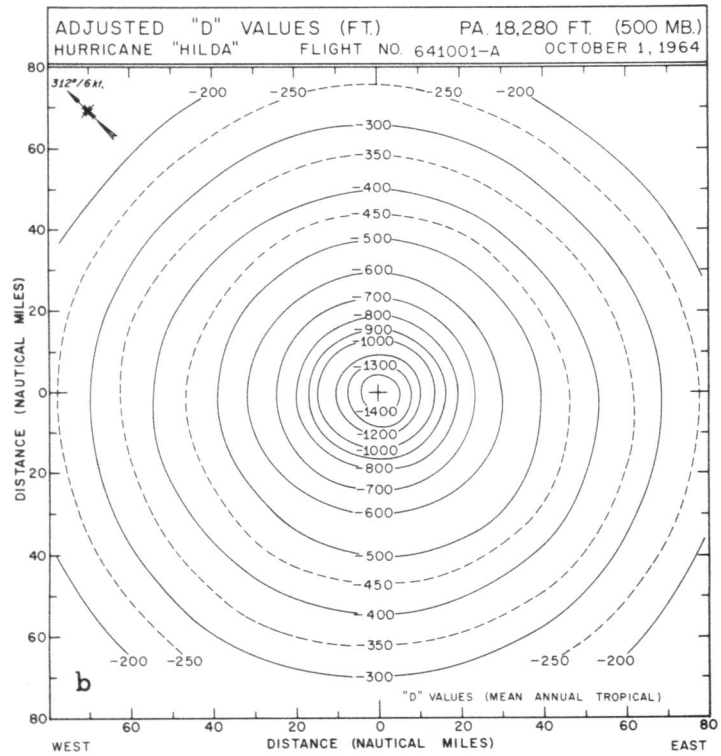

FIGURE 5.—*D*-values at (a) 900 mb., (b) 500 mb., and (c) 180 mb., the latter were partially constructed hydrostatically from the 500-mb. base.

part no abrupt discontinuities of lapse rate were introduced or necessary at the 900-mb. level because of these assumptions.

The lapse rates appeared to be consistently stable, particularly on the east side of the storm in the layer between 650 and 500 mb. Since the two temperatures defining this stability were measured from the same aircraft, no single correction applied consistently to this parameter would change the relative lapse rate.

It seems possible that the vortex thermometer's "wetting effect" might have contributed to exaggerating the stability since the 500-mb. pass was mainly above, while much of the 650-mb. pass was in the active precipitation. However, even if one raised the 650-mb. temperatures 2°C. on the eastern side of the storm a layer of marked stability would still remain. Moreover, the correction is presumably not applicable 60 mi. east of the center where the stability was quite well marked. The west side of the storm did not show the curious warmth at 500 mb. although on this side, too, the flight was not through any extensive areas of precipitation.

The dashed curves in figure 8 offer an appropriate moist adiabat for comparison with each sounding. In general, the closer the soundings with reference to the storm center, the warmer they were (particularly at higher levels). At most radii the lapse rate was close to moist (and also dry) adiabatic at the uppermost data point, 180 mb.

The composite eye sounding deserves mention. It shows that a stable layer existed from the "cloud base" to about the 750-mb. level, above which the lapse rate was briefly greater than moist adiabatic but in general very close to it. The structure was not unlike that in the eye

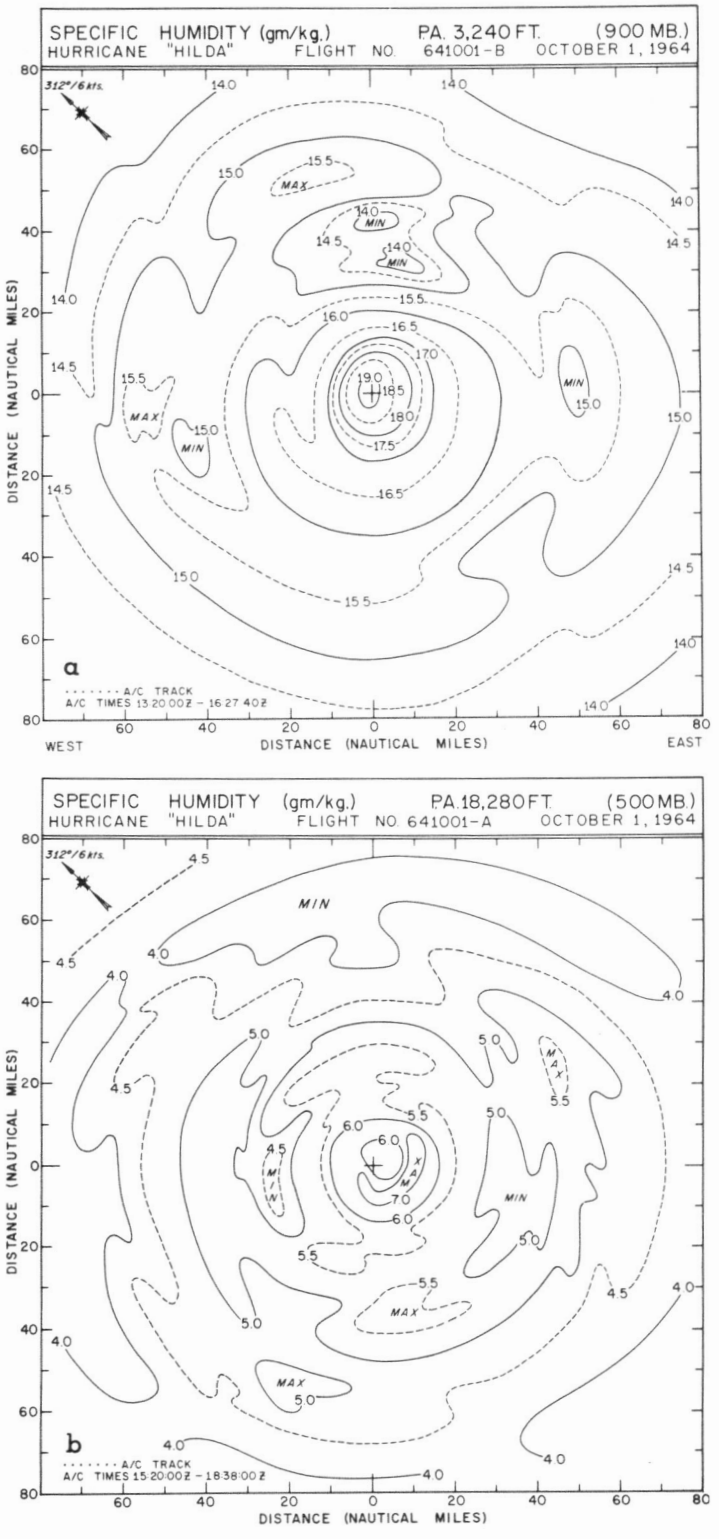

FIGURE 6.—Specific humidity at (a) 900 mb., showing again the maintenance of high specific humidity values through the eye of the storm; and (b) 500 mb., showing some tendency for lower eye-values.

of hurricane Arlene, as documented by Stear [21]. In that instance, the raob showed a very stable layer up to about 750 mb., a slightly greater than moist adiabatic lapse rate above this level to near 450 mb., above which the sounding was close to moist adiabatic. Thus, despite the hazards inherent in the time-space compositing technique, we felt that the eye-sounding was reasonably realistic. The upper level stability of the outer soundings may, of course, be attributed to the outflow of warm air after ascent in the core of the storm.

The vertical cross section of temperature anomaly (fig. 9) was prepared from the soundings shown in figure 8 using Jordan's [8] mean tropical sounding as normal. From 30 mi. outward below the 650-mb. level the anomalies were relatively insignificant. The strongest horizontal temperature gradients occurred in the eye wall at levels below 550 mb. Although the center of warm anomalies (+16°C.) was located at 250 mb., the horizontal gradients above 500 mb. in the outflow layer were much weaker than through the wall cloud at lower levels. The magnitude (+12°C.) of the anomaly that still persisted at 180 mb. was somewhat surprising. The tropopause may have been not only higher but also (probably) colder than normal, resulting in a rather strong vertical temperature gradient between 180 mb. and the tropopause level (Koteswaram [10]).

This anomaly pattern may be compared with that of hurricane Cleo, 1958 (LaSeur and Hawkins [12]). The upper flight level in that, much weaker, storm was at 239 mb. and the maximum recorded anomaly was +11°C. Although in the case of Hilda the maximum anomaly (+16°C.) was interpolated from the composited eye sounding, we felt that, barring marked upper level stable layers, there was not too much choice in drawing the eye sounding between 500 and 180 mb. In addition, the soundings were used to make hydrostatic computations that appeared to meet all consistency requirements. We feel, therefore, that although minor errors may have existed in the thermometry it was highly unlikely that any correction would be large enough to affect the major features of the pattern.

One further point of interest may be found in the sea level temperature gradient (heavy dashes at bottom of fig. 9). Since the temperatures were derived from the low level aircraft data extrapolated downward as already described, an interesting point arises as to whether or not the anomaly increase with decreasing surface pressure corresponds to that which would accompany the isothermal expansion proposed by Byers [2] as characteristic of the low level circulation of a hurricane. Inspection of the sea level "terminal" temperatures (fig. 8) shows that they all terminated at the same temperature within a quite acceptable tolerance of ±0.2°C. In view of the assumptions involved in processing the aircraft data and in the extrapolation to sea level this seems to be an acceptable independent confirmation that the in-spiralling air did indeed undergo an approximate isothermal expansion. It does not, however, prove that temperatures recorded in the low level pass itself were not too low because of extended flight through falling rain. Presumably

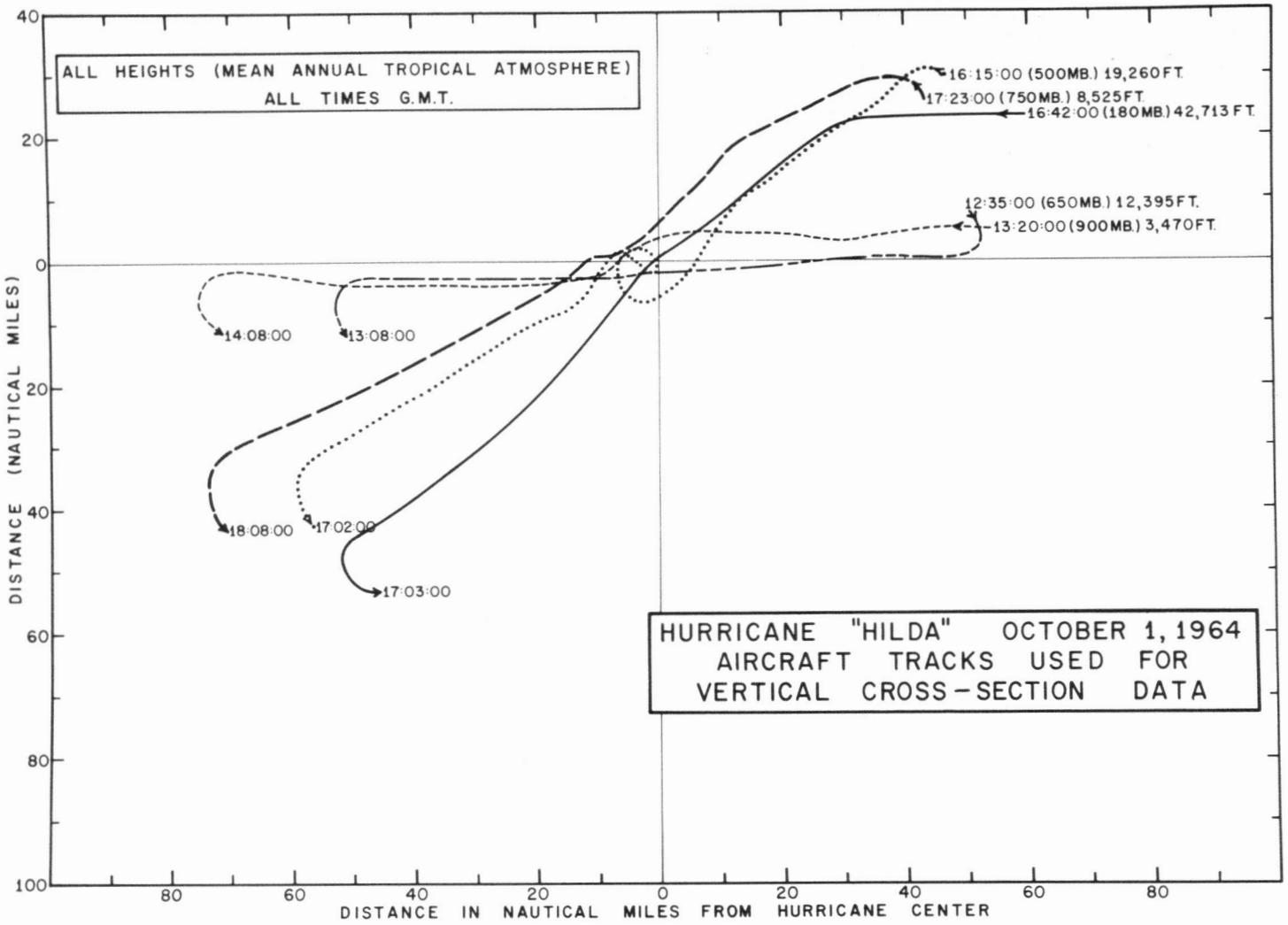

FIGURE 7.—The elevations, times, and relative horizontal tracks of the aircraft traverses used in constructing east-west vertical cross sections of hurricane Hilda.

a uniform positive correction applied to those temperatures would lead to a similar result but at a somewhat greater temperature.

D-VALUES

The D-value cross section (fig. 10) is, in part at least, a mirror image of the cross section of temperature anomaly. We may note that the D-value equals the radar or true altitude minus the pressure altitude (in the mean tropical atmosphere). Thus as one scans the cross section horizontally, the D-value variations indicate the change in altitude which that constant pressure surface underwent in hurricane Hilda. The five data levels were analyzed using the aircraft data plus hydrostatic computations to ensure vertical consistency. Only very minor adjustments of the aircraft D-value profiles were necessary after the profile had been positioned at the correct mean level. Gradient winds calculated from the derived field of values were found to be in general agreement with the observed winds. Maximum D-value horizontal gradients occurred in the lower levels in the eye wall near the radius of maximum winds.

As expected, the largest negative anomalies occurred in the eye at sea level. The magnitude of the negative anomalies decreased outward and upward, becoming generally positive above 200 mb. at just about all radii. The negative D-values, i.e., low pressures, are obviously attributable to the mass of warm light air above any given point. The air picks up sensible heat from the ocean in its isothermal expansion while spiralling in at low levels and also (as will be demonstrated) acquires even more energy in the form of latent heat. Much of this heated air rises in the wall cloud and spiral bands near the wall and then flows outward. The sea level pressure gradient is, in a sense, the integrated result of these processes. However, since the sea level pressure pattern itself is a significant factor in one of these processes there are manifest possibilities for the existence of a feedback mechanism.

WIND SPEEDS

The wind speeds (relative to the moving storm) are presented in a vertical cross section of hurricane Hilda

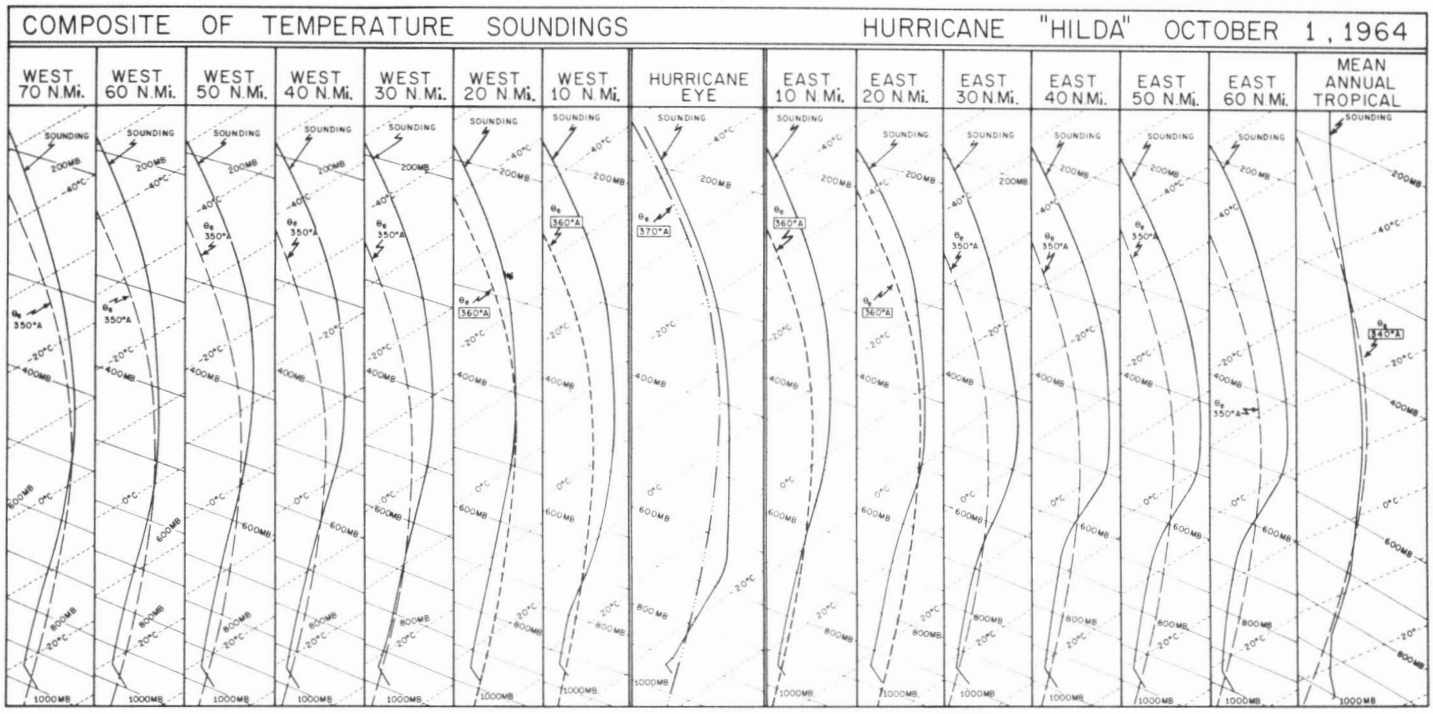

FIGURE 8.—Temperature soundings (solid line) at 10-n.mi. intervals across hurricane Hilda. The dashed line is an appropriate pseudoadiabat.

in figure 11. Maximum winds of 100 to 110 kt. were observed some 11 to 12 n.mi. east of the storm center. The pattern has been subjectively smoothed because time and space differences in compositing did not permit perfect coincidence of values. Maintenance of wind speeds with height (Hawkins [5]) was best demonstrated near and in the eye wall, where maximum winds of around 105 kt. on the east side at low levels gave way to a maximum of 48 kt. at 180 mb. On the west side of the storm the wind shear was even less, with low level values of around 95 kt. diminishing to around 55 kt. at 180 mb.

A careful check on the consistency of the wind and temperature field and on the balance and/or imbalance of these fields composited in the manner described (and smoothed subjectively) was made as follows:

If one considers the thermal wind equation in cylindrical coordinates and assumes steady state, frictionless motion, one can write:

$$\frac{\partial v_\theta}{\partial p}=\frac{-\frac{R}{p}\left(\frac{\partial T_v}{\partial r}\right)_p}{\left(f+\frac{2v_\theta}{r}\right)}.$$

Strictly speaking one should more properly consider, a) the total wind, b) the radius of trajectory curvature, and c) the shear of the curvature with pressure. However, the total winds are very similar to the actual tangential winds and one may for the moment assume that the curvature does not change with height in the inflow layer. With these reservations in mind computations were made through the inflow layer using the given equation for evaluating the shear over 5-n.mi. radial intervals and 100-mb. vertical increments.

Table 1 shows the results of these calculations for the 800-, 700-, 600-, and 500-mb. levels. The observed winds for 900 mb. are shown in the top row. The 800-mb. observed winds, the computed winds for this level, and the differences between the two occupy the next three rows. The differences are recorded as positive where the observed wind exceeds the computed and as negative otherwise. Differences are underlined once where they exceed 10 percent of the observed wind speed and are underlined twice where the differences exceed 20 percent. The computed winds are based on the observed 900-mb. winds (and the radial virtual temperature gradient), so that in effect all shears are cumulative from this level. Only six of the 96 values differ by 20 percent or more and 16 of the 96 differ by from 10 to 20 percent (of the observed wind speed). For the most part the differences between observed and computed speeds are small or negligible. Further, as the table shows, pluses predominate on the left (left side of the storm), negatives on the right (right side of the storm). If one considers the radius of trajectory curvature, it must be larger on the right of the direction of motion of the vortex and smaller on the left, an effect that would tend to diminish the magnitude of the positives on the left and the negatives on the right. The only conclusion possible from this array is that no consistent and strong deviations from the thermal wind relationship appear in the inflow layer.

Gray [4] has pointed out that the cumulus activity in a hurricane may play an ambiguous role in that the penetrative cumulonimbus towers which carry up and release the heat (making the storm warm core and weakening with height) also carry up higher momentum from the lower levels, tending to extend the strong lower level

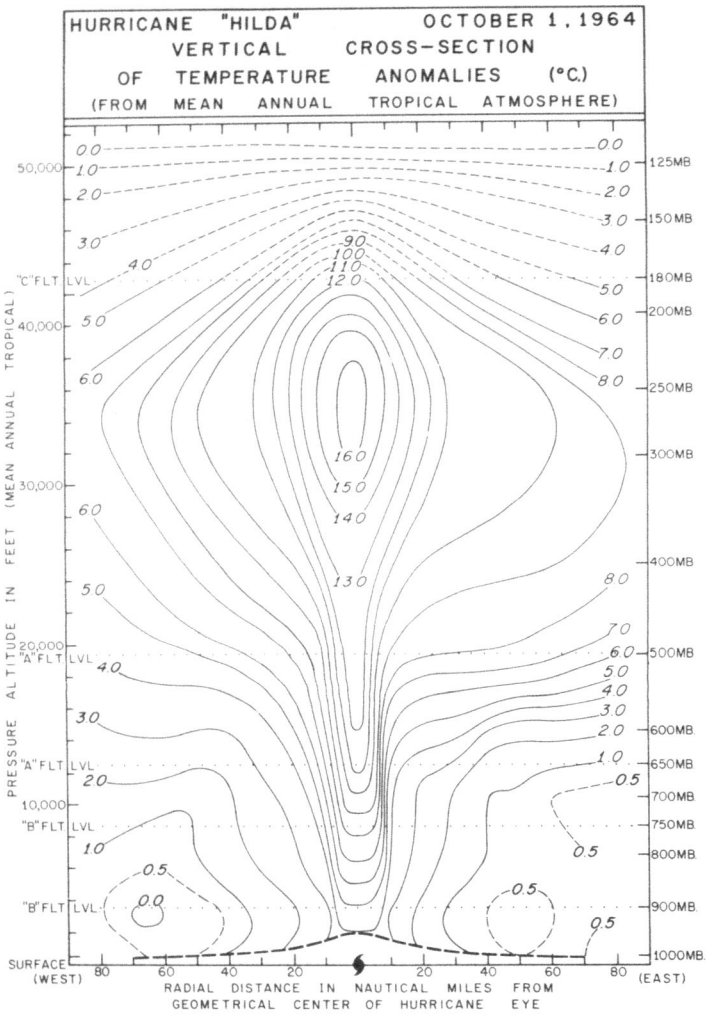

FIGURE 9.—Vertical cross section of temperature anomaly prepared from the soundings presented in figure 8.

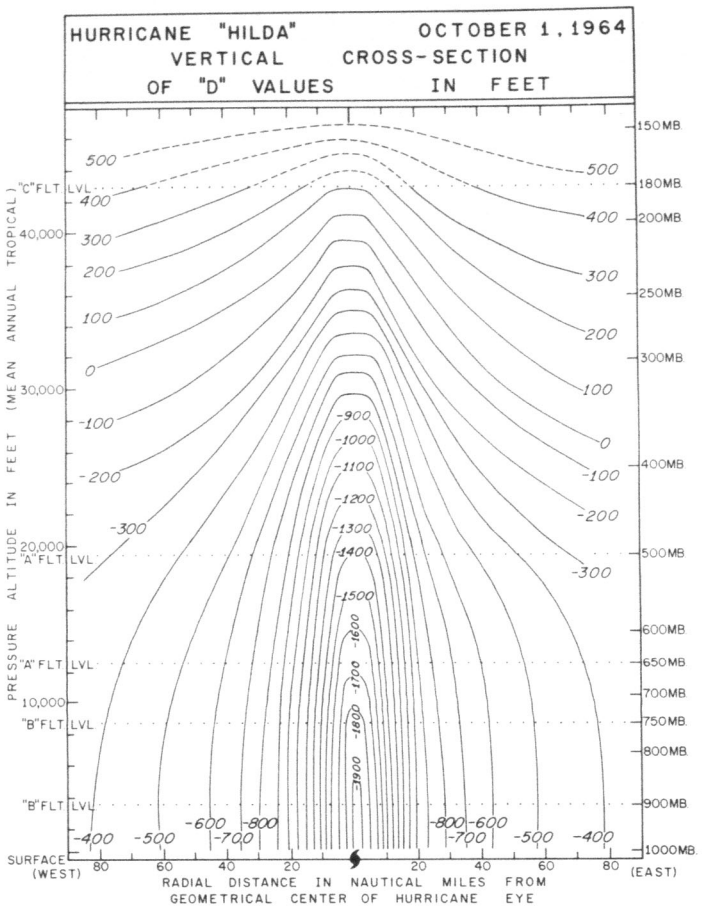

FIGURE 10.—Vertical cross section of *D*-values (from the mean tropical atmosphere).

circulation to higher elevations. While momentary excesses of wind over gradient may well exist in such gusts or bubbles, it seems unlikely that over any appreciable time period or any extensive area excessive imbalances can be maintained. Nevertheless, the dual opposing roles that the cumulus plays have been well posed by Gray.

RADAR ECHOES

The radar cross section (fig. 12) has been prepared by scanning the RDR-1D (3.2 cm.) vertical cross-section radar on each of the four, lower level flights. The flight track was stippled when the plane appeared to be in an active echo. Because of the extremely short ranges (5 to 10 mi. on the average) and the small antenna, spurious echoes from side lobes and general clutter made interpretation of the scope exceedingly difficult. The major portion of the area under surveillance was characterized by precipitation falling from the bright band which was, for the most part, quite well defined. Thus the radar echo tops were generally even and stratiform. The major exception to this condition was in the wall cloud. On the eastern (right hand) side of the storm echoes rose to about 200 mb., i.e., around 40,000 ft. This was the only area of the storm in which really deep, vigorous ascent appeared to mount well into the upper troposphere. The percentage area covered by active cumulus or cumulonimbus towers was certainly not greater than the generally small figure usually allotted to this activity. The visible cloud, of course, surmounted the echoes in all areas, for the jet aircraft at 180 mb. was in cirrus throughout most of its transit of the storm.

On a lower level of the diagram we have depicted in thick lines the areas where the APS-20 (10 cm.) radar suggested the more prevalent major rain bands were located. These were composited over some period of time from the two APS-20 films available. In view of the differences in the radars and in the method of compositing it is not surprising that there are differences in the two composite presentations. Since only the stronger bands are distinguishable on the APS-20 (10 cm.) one should expect the echo area to be smaller than the precipitation area derived using the 3-cm. set. The most unusual feature of the figure is the length of flight through rain at the lowest level. Presumably the hardest rain occurred in the limited areas of the 10-cm. radar echoes.

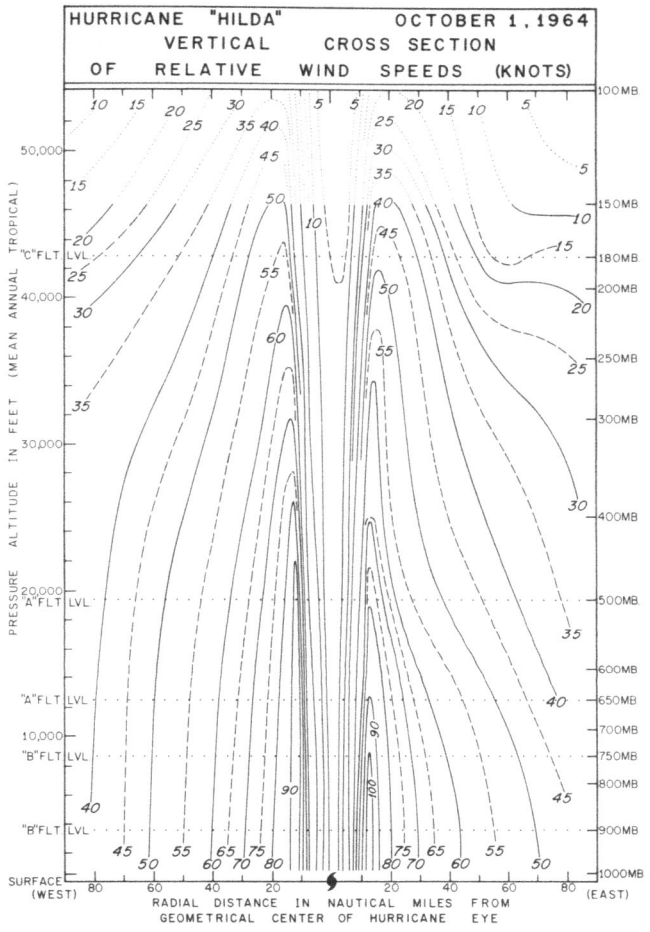

FIGURE 11.—Vertical cross section of wind speeds relative to the moving hurricane eye.

5. FEATURES OF THE MASS FLOW FIELD

RADIAL MASS FLOW

We have already mentioned the hazards involved in compositing observations around the moving storm. One of the parameters most sensitive to these uncertainties is the radial velocity. Nevertheless, if we wish to investigate certain classes of problems, we have to estimate radial velocities as best we can. The various budget studies demand reasonable values of the radial velocity (v_r) and several techniques have been devised for dealing with the problem.

This most important single item in the budget studies, the distribution of radial velocities with height and radius, is shown in figure 13. Mean values of v_r (relative to the moving storm) were acquired at each flight level for every 10-n.mi. radial interval by reading wind direction and speed along radials constructed at 30° intervals from each of the horizontal field analyses and then computing the radial components. These values were plotted on a diagram (fig. 13) for purposes of analysis. Since no data were available below 900 mb. some decision had to be made as to the general shape of the curve at low levels.

We have assumed that the low level inflow increases with decreasing elevation through *most* of the friction layer, an assumption similar to those made by other researchers (Miller [14], [15], [16]; Riehl and Malkus [19]; Rosenthal [20]). The inflow layer itself was fairly well defined by these means and was shown to extend from the surface to about 650 mb.; there was a slight suggestion, but no conclusive evidence, that the inflow layer de-

TABLE 1.—*Wind speeds (kt.), observed and computed (from the radial thermal gradient)*

Radial Distance	(n.mi. left)	67.5	62.5	57.5	52.5	47.5	42.5	37.5	32.5	27.5	22.5	17.5	12.5
Level (mb.)													
900	Obs.	42	45	47	49	51	54	58	62	67	72	79	87
800	Obs.	41	44	47	49	51	54	57	61	66	70	77	87
	Comp.	40	42	45	47	49	50	54	60	66	70	77	84
	Diff.	+1	+2	+2	+2	+2	+4	+3	+1	0	0	0	+3
700	Obs.	41	44	46	48	51	53	56	60	65	70	77	85
	Comp.	40	43	41	43	46	46	51	58	64	67	75	78
	Diff.	+1	+1	+5	+5	+5	+7	+5	+2	+1	+3	+2	+7
600	Obs.	40	43	46	48	50	52	55	58	63	68	75	85
	Comp.	37	44	40	40	43	41	48	55	60	62	69	72
	Diff.	+3	−1	+6	+8	+7	+9	+7	+3	+3	+6	+6	+13
500	Obs.	39	42	44	47	49	51	53	56	60	67	72	85
	Comp.	32	41	40	36	35	38	44	52	55	55	62	65
	Diff.	+2	+1	+4	+11	+14	+13	+9	+4	+5	+12	+10	+20
Radial Distance	(n.mi. right)	12.5	17.5	22.5	27.5	32.5	37.5	42.5	47.5	52.5	47.5	62.5	67.5
Level (mb.)													
900	Obs.	107	91	82	77	72	68	65	63	61	59	57	56
800	Obs.	105	90	82	75	70	67	64	62	60	58	56	54
	Comp.	104	90	79	75	68	67	64	62	59	60	58	56
	Diff.	+1	0	+3	----------	+2	0	0	0	+1	−2	−2	−2
700	Obs.	95	87	80	73	68	64	62	60	58	56	55	51
	Comp.	100	87	77	72	65	63	62	61	57	57	57	56
	Diff.	−5	0	+3	+1	+3	+1	0	−1	+1	−1	−2	−5
600	Obs.	85	83	75	68	63	61	58	57	54	52	50	47
	Comp.	93	83	75	70	63	58	55	59	53	56	56	56
	Diff.	−8	0	0	−2	0	+3	+3	−2	+1	−4	−6	−9
500	Obs.	77	75	65	60	58	55	53	52	50	47	45	43
	Comp.	87	80	72	69	61	55	48	56	51	55	56	53
	Diff.	−10	−5	−7	−9	−3	0	+5	−4	−1	−8	−11	−10

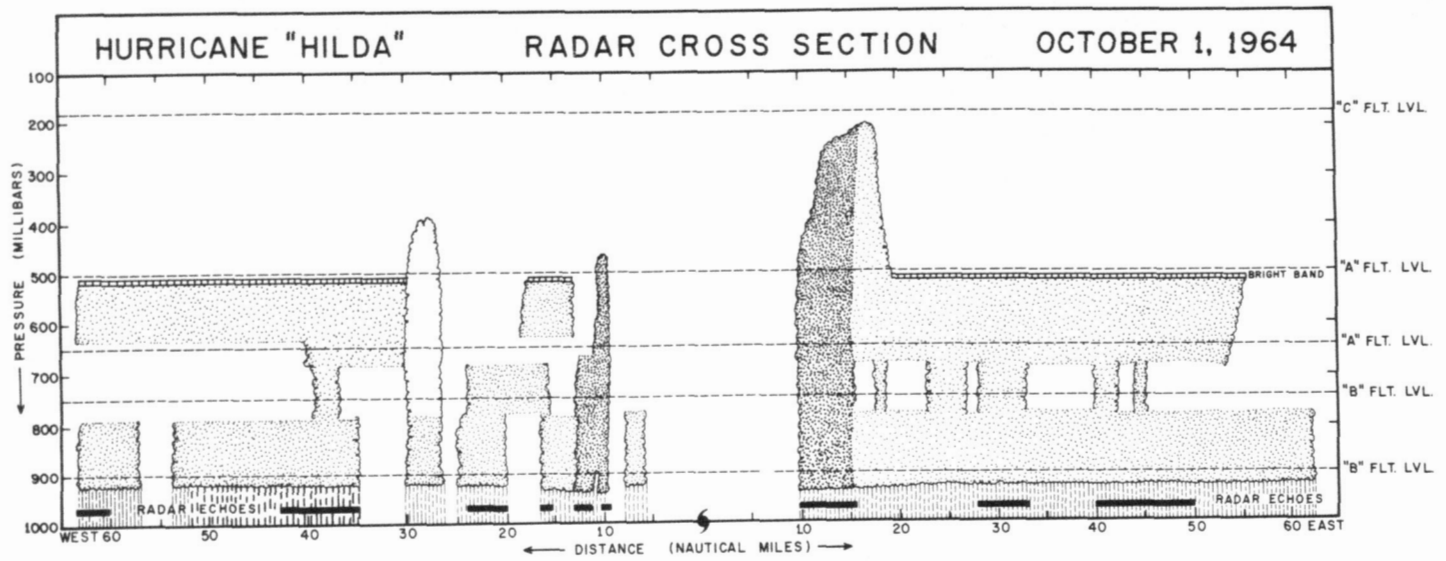

FIGURE 12.—Vertical cross section of radar echoes. Each flight level is stippled where the plane appeared to be in an active 3-cm. radar echo. The bright band is indicated where observed by the RDR-1D vertical height-finding radar. The lower, thick lines labeled "radar echoes" are the more stable and well-marked bands composited from the 10-cm. APS-20 film as representative of the band structure over the major portion of the period of flight. Darker stippling has been used to represent the major wall cloud and its more active cumulus character.

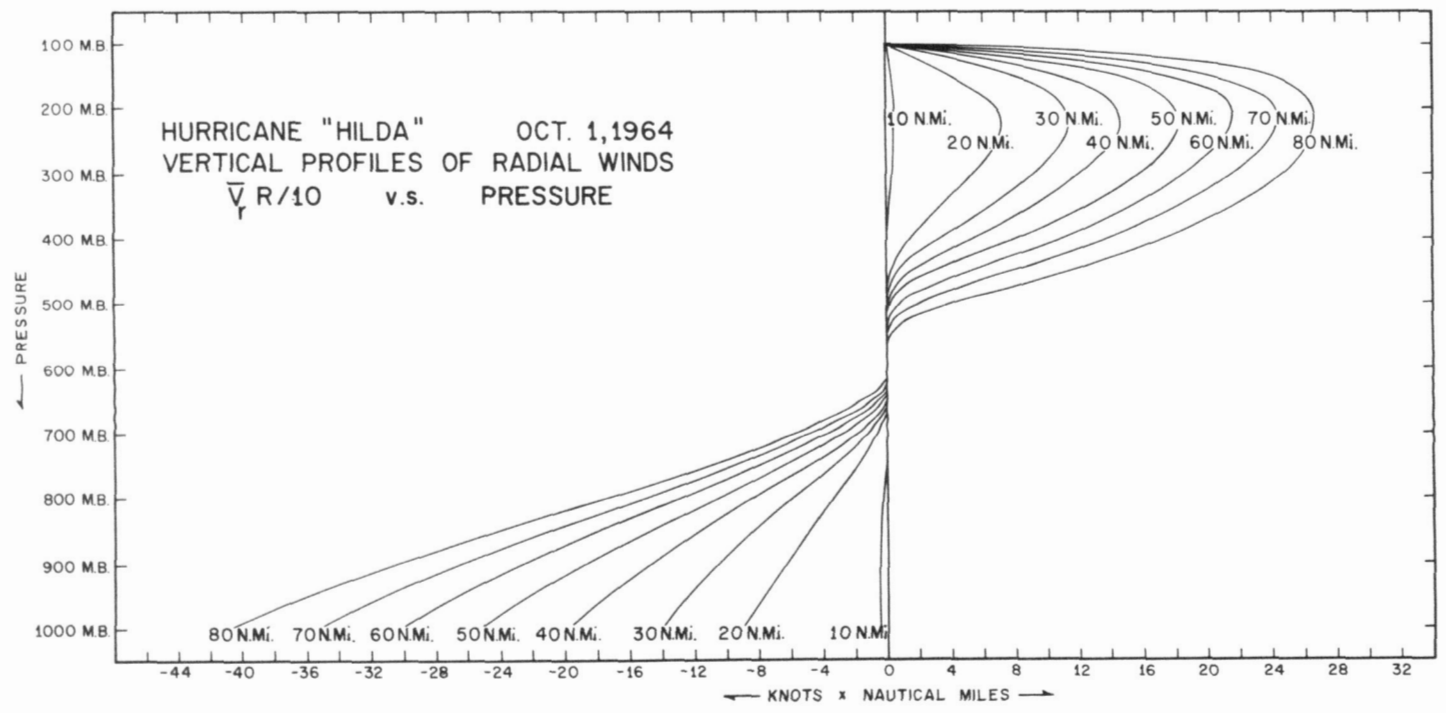

FIGURE 13.—Curves of radial velocity (in the form of $rv_r/10$) against pressure for various radii. Mass balance is required at every radius.

scended with decreasing radius. In the layer from 650 to 500 mb., radial motion was weak or nonexistent, and at 500 mb. the lower extremes of the outflow layer were barely visible.

The curves in the outflow layer were drawn under the assumptions that 1) the radial flow goes to zero at 100 mb. and 2) the mass outflow across any given radius just balances the mass inflow across the radius. Although the values of the inflow at 180 mb. obtained from the flight data were most helpful, they were above the maximum (in elevation) and allowed considerable flexibility in the shape of the curve. We have also assumed that gradations in the radial flow from one radius to another would be in the form of gradual transitions rather

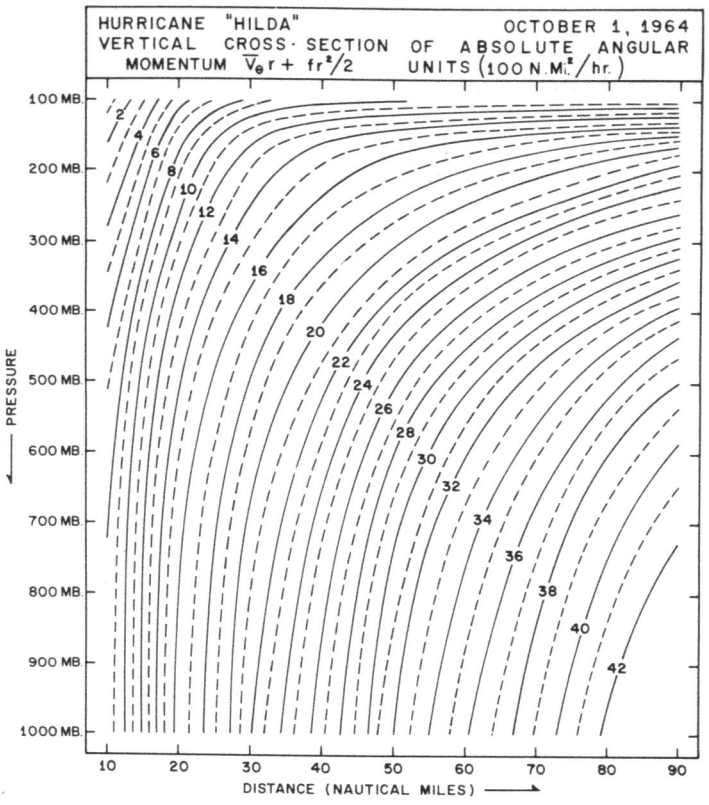

FIGURE 14.—Vertical cross section of absolute angular momentum for tangential winds that have been averaged azimuthally about the moving storm.

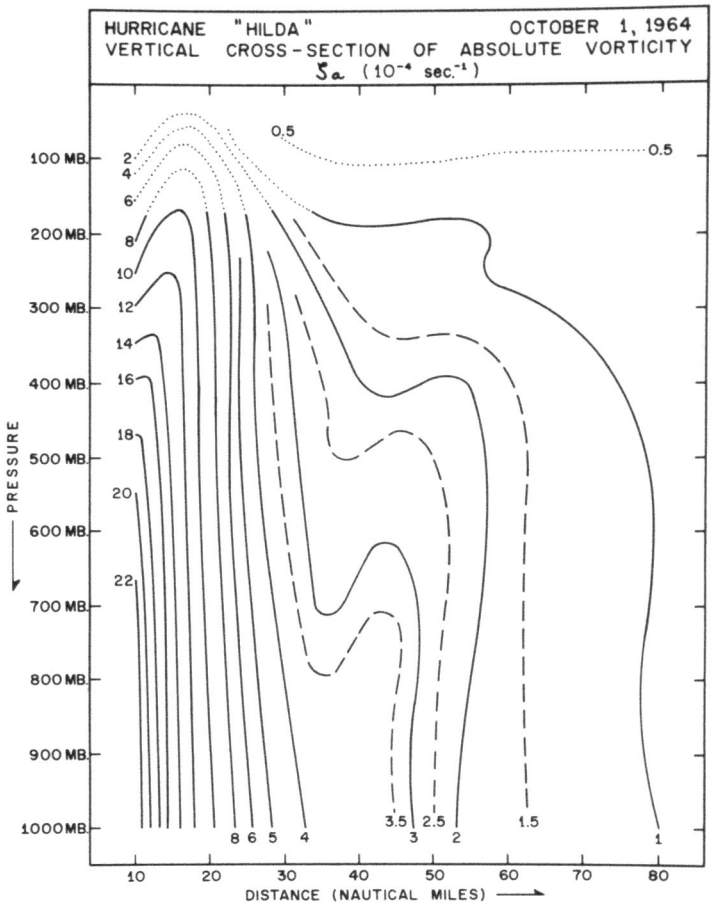

FIGURE 15.—Vertical cross section of absolute vorticity for the mean tangential relative winds.

than in the form of alternate annular rings representing convergence, divergence, etc. All these criteria could be met if one assumed that the computed mean radial velocities were accurate to ± 1 kt., i.e., that the curves as drawn did not depart from the appropriate data points by more than the equivalent difference of 1 kt. in the mean radial flow. Any more explicit reliance on the mean "observed" radial velocities would be unrealistic.

The radial wind profiles are the most important single factor in all budget computations. The curves have been drawn with the greatest possible care and the equal areas were measured by means of a planimeter. Some further documentation was available at 900 mb. Figure 1a shows that a closed hexagonal figure was flown about the storm at this level. The mean radial velocity of the 5,500 observations gathered around this closed path at 900 mb. was plotted on the radial wind profiles at the mean radial distance and has been drawn to exactly. Note that in both the inflow and outflow layers these radial velocities were rather small compared with those used by other investigators and in general were about half the normally assumed values.

MEAN TANGENTIAL FLOW

In a manner similar to that employed in computing the mean (relative) radial velocities, the mean (relative to the moving storm) tangential velocities (v_θ) were also computed. From these winds we constructed cross sections of absolute angular momentum (fig. 14) and of absolute vorticity (fig. 15).

The absolute angular momentum,

$$M = v_\theta r + fr^2/2,$$

of a parcel of air in the inflow layer obviously decreased as the parcel spiraled inward. This decrease, directly attributable to the drag exerted on the sea surface by the moving air, was imparted to the ocean. At upper levels in the outflow layer, the absolute angular momentum of the parcels was more likely to be conserved. Here the isopleths become almost horizontal, particularly at the higher levels. Figure 14 suggests that the air which penetrated farthest inward lost more of its momentum than other parcels and may have risen quite high before significant outward motion took place. It seems doubtful, however, that the parcels followed exactly along the isopleths; turbulent exchange with adjacent parcels of different value would tend to alter the absolute angular momentum value with which the parcel traveled along on its outward trajectory.

The mean cross section of absolute vorticity,

$$\zeta_a = \frac{v_\theta}{r} + \frac{\partial v_\theta}{\partial r} + f,$$

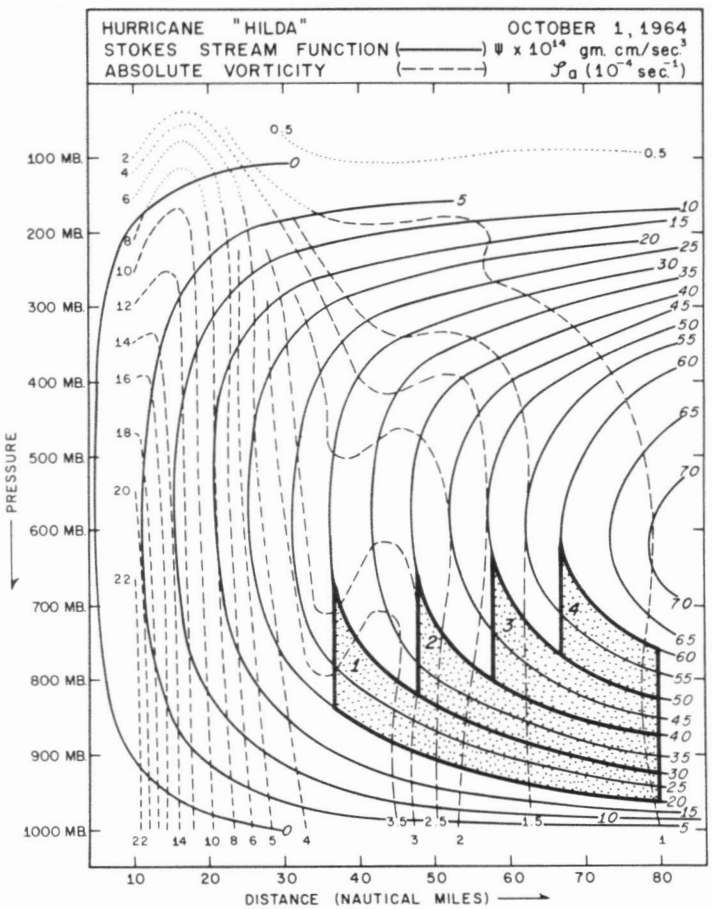

FIGURE 16.—Solid lines are Stokes' stream function superimposed on (dashed) lines of absolute vorticity. Selected streamtubes are indicated by 1, 2, etc.

TABLE 2.—*Conservation of potential vorticity*

	Streamtube			
	1	2	3	4
ζ_{a_2}/ζ_{a_1}	3.3	3.4	2.1	1.6
$\Delta p_2/\Delta p_1$	3.3	3.4	3.3	2.4

is presented in figure 15. Most of the values were greater than 10^{-4} sec.$^{-1}$ and near the eye wall values of the order of 10^{-3} sec.$^{-1}$ were encountered. Riehl and Malkus [19] have pointed out that while frictional influences undoubtedly affect the vorticity field, the major configuration of the vorticity field (and the absolute angular momentum field) is presumably still linked to the distribution of convergence and divergence so that, in the first approximation, the theorem of potential vorticity may hold. If so,

$$\frac{\zeta_{a_2}}{\zeta_{a_1}}=\frac{\Delta p_2}{\Delta p_1},$$

where Δp is the pressure depth of the column considered.

We have computed Stokes' stream function for the radial and vertical motions that follow from the radial wind profiles. If the equation of continuity is employed,

$$\frac{\partial \omega}{\partial p}+\frac{1}{r}\frac{\partial (rv_r)}{\partial r}=0$$

from which

$$\omega=-\frac{1}{r}\frac{\partial \psi}{\partial r},$$

and

$$rv_r=\frac{\partial \psi}{\partial p}.$$

The stream function was computed from the latter expression and the streamtubes are shown as continuous lines in figure 16. A number of the streamtubes were used to evaluate the conservation of potential vorticity. Table 2 shows that within the inflow layer there was a tendency to conservation. In the very lowest layer where frictional effects were strongest there was little conservation. In the layers of streamtubes from about 950 mb. to 850 mb., however, potential vorticity was conserved as it probably also was above this level, although uncertainty in evaluating the terminal pressure depths cast some doubt on the numerical evaluations.

As figure 16 shows, in the upper portions of the outflow layer the streamtubes are very nearly parallel to the lines of constant angular momentum. There seems every reason to expect that absolute angular momentum is conserved at these levels and that some turbulent mixing is the only modifying process.

6. BUDGET OF ABSOLUTE ANGULAR MOMENTUM AND EVALUATION OF THE SURFACE STRESS

The mean flux of absolute angular momentum (M) was computed for the "mean symmetrical" hurricane. Figure 17 presents the results of these calculations, which are basically similar to the computations of Riehl and Malkus [19] and Miller [14]. The horizontal fluxes in figure 17 were calculated at 10-n.mi. intervals radially and 100-mb. intervals vertically, i.e., flux$=2\pi r\overline{Mv_r}\ \Delta p/g$, where $\overline{M}$ and $\overline{v_r}$ are the appropriate *mean values* of absolute angular momentum and radial velocity.

The momentum extracted by the ocean was computed in two ways and the results are tabulated immediately below 1000 mb. in figure 17. Values in parentheses were derived using the net horizontal fluxes into and out of the annular volumes from sea level up to the 100-mb. level. In each volume there was a net excess representing the momentum lost to the ocean. The weakness in this procedure lies in the fact that the outflow layer data were very sparse and the maximum outflow occurred below

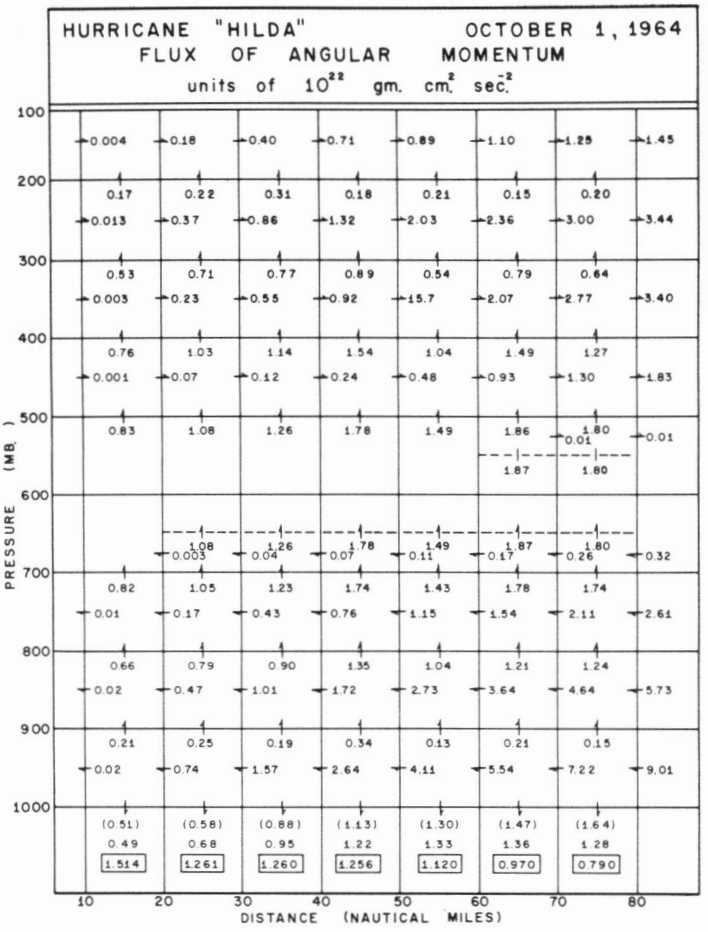

FIGURE 17.—Flux of angular momentum for the "mean symmetric" hurricane Hilda. In the lower boxes, numbers in parentheses are momentum losses to the sea computed to the top of the atmosphere (100 mb.). Immediately below are the same losses computed on the basis of the better defined inflow layer data. Enclosed in the boxes are momentum losses per unit area in units of 10^8 gm. sec.$^{-2}$

the upper observational level, in the very region where the vertical gradient of absolute angular momentum was quite strong. This meant that horizontal fluxes in the outflow layer could be materially altered by relatively minor shifts in the rv_r profile aloft. For these reasons, an alternate method was used based only on data from the better defined inflow layer. The resulting values are given immediately below the estimates in parentheses. The differences in most cases were of the order of 10 percent or less.

As one might expect, the total angular momentum lost to the ocean was greater in the outer volumes and decreased inward. This is attributable to the greater ocean surface area in the outer volumes, which apparently more than compensates for the increasing wind speeds and greater drags in the inner volumes. The enclosed figures given at the bottom of figure 17 are the momentum losses per square centimeter ($\times 10^8$ gm. sec.$^{-2}$) in each of the annular rings. These show that the rate at which angular momentum was extracted per unit area increased as the radial distance decreased, resulting in greater loss per unit area at higher wind speeds.

With the data at hand, estimates were then made of the surface stresses by means of which the angular momentum was transferred to the ocean. In the more conventional approach, the tangential equation of motion in cylindrical coordinates may be written:

$$\frac{dv_\theta}{dt}=\frac{\partial v_\theta}{\partial t}+v_\theta\frac{\partial v_\theta}{r\partial\theta}+v_r\frac{\partial v_\theta}{\partial r}+w\frac{\partial v_\theta}{\partial z}=-fv_r-\frac{v_rv_\theta}{r}-\frac{1}{\rho}\frac{\partial p}{r\partial\theta}+\frac{1}{\rho}\frac{\partial\tau_{\theta_z}}{\partial z},$$

where lateral frictional effects have been ignored and the symbols are conventional, with τ_{θ_z} defined as the shearing stress in the θ–z plane. If we assume a steady state relative to the moving system and symmetry, i.e., in effect that the tangential gradients of p and v_θ are negligible, we may write:

$$\frac{1}{\rho}\frac{\partial\tau_{\theta_z}}{\partial z}=v_r\left(\frac{\partial v_\theta}{\partial r}+\frac{v_\theta}{r}+f\right)+w\frac{\partial v_\theta}{\partial z},$$

or

$$-\int_{p_0}^{p_H}\frac{\partial\tau_{\theta_z}}{\partial p}dp=\tau_{\theta_0}-\tau_{\theta_H}=\int_{p_0}^{p_H}v_r\zeta_a\frac{dp}{g}+\int_{p_0}^{p_H}w\frac{\partial v_\theta}{\partial z}\frac{dp}{g},$$

where p_0 is the surface pressure, p_H is the pressure at the top of the inflow layer (where $\overline{v}_r$ is zero and τ_{θ_H} is usually assumed negligible). The second term on the right has been variously estimated at around 10 percent of the first term and is usually neglected.

An equivalent expression can be derived, which involves the absolute angular momentum, M, in the place of the absolute vorticity:

$$\frac{dM}{dt}=\frac{d}{dt}\left(v_\theta r+\frac{fr^2}{2}\right)=r\frac{dv_\theta}{dt}+v_\theta v_r+rfv_r=-rg\frac{\partial\tau_{\theta_z}}{\partial p};$$

also,

$$\frac{dM}{dt}=\frac{\partial M}{\partial t}+v_\theta\frac{\partial M}{r\partial\theta}+v_r\frac{\partial M}{\partial r}+\omega\frac{\partial M}{\partial p}+M\left(\frac{\partial v_r}{\partial r}+\frac{v_r}{r}+\frac{\partial\omega}{\partial p}\right)--=rg\frac{\partial\tau_{\theta_z}}{\partial p};$$

or,

$$\int_{p_H}^{p_0}-rg\frac{\partial\tau_{\theta_z}}{\partial p}dp=\int_{p_H}^{p_0}\frac{1}{r}\left[\frac{\partial}{\partial r}\left(rv_rM\right)+\frac{\partial}{\partial p}\left(\omega Mr\right)\right]dp;$$

and,

$$\tau_{\theta_0}-\tau_{\theta_H}=\frac{1}{r^2}\int_{p_0}^{p_H}\frac{\partial}{\partial r}\left(rv_rM\right)\frac{dp}{g}+\frac{\omega_HM_H}{rg}$$

where use has been made of the appropriate expression for the equation of continuity. In this latter form of the equation for the stress, we can make ready use of the rv_r curves (fig. 13) and of the angular momentum profile (fig. 14). The vertical velocities were calculated from the rv_r curves. If instead of integrating only over the inflow layer, one integrates to the top of the atmosphere, τ_{θ_H} becomes negligible. However, uncertainties arise because of the lack of data at upper levels.

TABLE 3.—*The tangential shearing stress computed in four different ways for 10-n.mi. annular rings centered on 15, 25, etc. n.mi.*

HURRICANE "HILDA" STRESS UNITS DYNES / CM.² OCTOBER 1, 1964							
RADIUS NAUTICAL MILES	15	25	35	45	55	65	75
$\tau_{\theta_0} = \frac{1}{r^2}\frac{\partial}{\partial r}\int_{p_0}^{p_H} v_r r M \frac{dp}{g} + \frac{\omega_H M_H}{rg}$	52.4	27.0	19.3	15.0	11.0	8.0	5.7
$\tau_{\theta_0} = \frac{1}{r^2}\frac{\partial}{\partial r}\int_{p_0}^{100} v_r r M \frac{dp}{g}$	57.2	22.7	18.0	13.9	10.7	8.7	7.3
$\tau_{\theta_0} = \int_{p_0}^{p_H} v_r \mathcal{J}_a \frac{dp}{g}$	36.3	24.3	15.3	15.9	9.7	6.2	5.7
$+\left(\int_{p_0}^{p_H} w \frac{\partial v_\theta}{\partial z}\frac{dp}{g}\right)$	(7.2)	(3.0)	(2.4)	(1.9)	(1.2)	(0.9)	(0.6)
	43.5	27.3	17.7	17.8	10.9	7.1	6.3
$\tau_{\theta_0} = \int_{p_0}^{100} v_r \mathcal{J}_a \frac{dp}{g}$	15.4	8.8	8.4	10.3	3.6	1.9	2.2
$+\left(\int_{p_0}^{100} w \frac{\partial v_\theta}{\partial z}\frac{dp}{g}\right)$	(52.5)	(15.0)	(10.7)	(7.9)	(6.6)	(5.1)	(4.2)
	67.9	23.8	19.1	18.2	10.2	7.0	6.4

TABLE 4.—*Drag coefficients computed from the indicated stress values*

HURRICANE "HILDA" OCTOBER 1, 1964 DRAG COEFFICIENTS AND TANGENTIAL SURFACE STRESSES COMPUTED FROM THE ANGULAR MOMENTUM BALANCE							
RADIUS (N.Mi.)	10-20	20-30	30-40	40-50	50-60	60-70	70-80
Cd x 10^{-3}	3.56	2.17	1.99	1.84	1.58	1.42	1.20
$\overline{\tau}_{\theta_0}$ (Dynes / Cm.²)	52.44	26.98	19.30	15.00	11.00	8.04	5.68

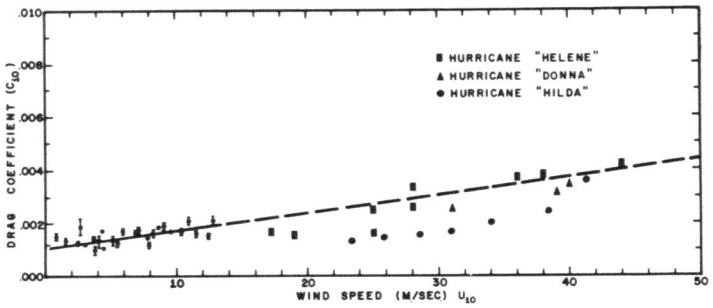

FIGURE 18.—Drag coefficients for hurricane Hilda plotted against a background of other hurricane and lower speed determinations (after Miller [17]).

We evaluated the surface stress, τ_{θ_0}, (assuming $\tau_{\theta H}$ negligible) in four "different" ways. That is, we integrated each of the expressions through the inflow layer and also from the surface to the top of the atmosphere (assumed to be 100 mb.). The results of these numerical integrations are presented in table 3. The top line represents the most convenient expression to evaluate computed through the inflow layer where the data were best. The second line evaluated these same expressions from the surface to 100 mb. In general the agreement appears to be fairly good. The data were of such quality that we do not feel the differences in the τ_{θ_0} values reflect the value of τ_{θ_H} in any significant way.

The lower two lines of table 3 present analogous calculations for τ_{θ_0} using the expression involving the absolute vorticity and including the frequently neglected shear term. In the inflow layer the shear term was about 10 percent of the vorticity advection term except in the smallest annulus. When evaluation was made to the top of the atmosphere the shear term became, in general, the dominant term. With the exception of the innermost annular ring, the final values are reasonably similar. For reasons already stated, the evaluation through the well-documented inflow layer (top line) was selected as "best" and these values were used in determining the momentum exchange coefficient. These calculations involved the mean transport terms only.

The stress averaged around 6 dynes/cm.² in the outer ring where winds were about 24 m./sec., rising to some 52 dynes/cm.² in the innermost ring where winds averaged about 41 m./sec. Through use of the empirical formula

$$\tau_{\theta_0} = \rho C_d v_\theta V \approx \rho C_d v_\theta^2$$

where V is the total wind (as contrasted to the tangential surface wind) the drag coefficients (table 4) were evaluated for the various annular rings and corresponding wind speeds. The dimensionless drag coefficients ranged in value from 0.0012 to 0.0036 and have been plotted against wind speed (large solid circles) in figure 18. The drag coefficients for higher wind speeds from hurricanes Helene and Donna were obtained by Miller [16], who also presented estimates for lower wind speeds taken from a summary by Deacon and Webb [3]. The values for hurricane Hilda appear overall to be somewhat low at intermediate speeds but agree with Miller's estimates at maximum speed. They suggest a curvilinear dependence of drag coefficient on wind speed rather than the linear relation (dashed line, fig. 18) suggested by Miller. Palmén and Riehl [18] used the composited mean hurricane data of Hughes [7] and E. Jordan [9] to estimate drag coefficients. Their values ranged from 1.1×10^{-3} to 2.1×10^{-3} for winds that varied from 6 to 26 m./sec. The technique they used also employed an angular momentum budget.

In working with the data of hurricane Daisy, Riehl and Malkus [19] used an assumed constant drag coefficient of 2.5×10^{-3} inside the 80-n.mi. radius to estimate the transfer of angular momentum into the ocean. They found that while the disturbance was in the tropical storm stage the angular momentum balance was reasonably satisfied without transfer by lateral stresses. When the hurricane reached maximum intensity, however, balance was achieved only through sizable exports by means of lateral stresses.

The computations just cited also included estimates of the lateral transports by eddies. The day when hurri-

TABLE 5.—*For the indicated radial intervals the following quantities are listed in order: the air-sea temperature difference, the air-sea (saturation at sea temperature) specific humidity difference, mean wind speed, exchange coefficients, sensible heat transfer, latent heat transfer, the Bowen ratio, and outgoing radiant heat energy.*

HURRICANE HILDA OCTOBER 1, 1964 CALCULATIONS OF EXCHANGE OF SENSIBLE AND LATENT HEAT AND OUTGOING RADIATION							
RADIAL INTERVAL (N.Mi.)	10–20	20–30	30–40	40–50	50–60	60–70	70–80
$T_0 - T_A$ (°C.)	4.9	5.1	5.2	5.2	5.1	5.0	5.0
$q_0 - q_A$ (g/Kg)	9.5	10.4	10.9	11.2	11.4	11.5	11.6
V (KT.)	69.4	63.9	56.3	51.6	47.8	43.2	39.5
$C_h = C_e = C_d$ ($\times 10^3$)	3.56	2.17	1.99	1.84	1.58	1.42	1.20
$Q_s \times 10^{12}$ Joules/sec.	2.11	1.82	2.06	2.15	2.24	2.35	2.48
$Q_e \times 10^{12}$ Joules/sec.	10.17	9.23	10.74	11.56	14.77	13.47	14.34
r_b	0.21	0.20	0.19	0.19	0.15	0.17	0.17
$R_A \times 10^{12}$ Joules/sec	.44	.73	1.02	1.30	1.59	1.88	2.17

cane Daisy was at maximum strength the eddy transport of angular momentum was outward and was approximately 10 percent of the total import at the given radial distance. In the case of hurricane Hilda we had available the circumnavigation data at 900 mb. at a mean radial distance of about 50 n.mi. The inward angular momentum transport by the mean mass flow for the 950- to 850-mb. layer at this distance was 3.6×10^{22} gm. cm.^{2} sec.$^{-2}$; the eddy transport corresponding to this mean was 1.4×10^{21} gm. cm.^{2} sec.$^{-2}$, directed outward. Thus, the eddy transport was about 5 percent of the mean and in a direction opposite to that of the mean transport.

7. BUDGET OF TOTAL EFFECTIVE ENERGY

The phrase "total effective energy," H, is used here to indicate the total energy of the parcel less the kinetic energy. Since even in a hurricane the kinetic energy is but a small fraction of the total energy, H is a useful concept although a misnomer in the sense that for some purposes the energy of the wind is the effective portion of the kinetic energy.

Computations of the exchanges of sensible and latent heat at the ocean surface involved the following assumptions and procedures:

1) The exchange coefficients for sensible heat, C_h, and moisture, C_e, were assumed identical with that for momentum, C_d.

2) The sea surface temperature, T_0, was assumed to be a uniform 30° C. This warmth before the passage of Hilda has been well documented by Leipper [13]. Whether one is justified in assuming a uniform temperature that applies equally to the front and rear of the storm appears dubious in the light of Leipper's findings. (The recent advent of reliable infrared thermometers will provide a handy tool for further research in this area.)

3) The air temperature, T_a, at the various radii was derived from the soundings shown in figure 8 by extrapolation from the 900-mb. flight temperatures, as previously described.

4) With the ocean temperature and pressure given, the saturation mixing ratios at the sea surface, q_0, was computed using a tephigram. The actual mixing ratio of the air, q_a, was similarly obtained by tephigram on the basis of the 900-mb. data level under the assumptions previous listed.

5) The vertical transports of sensible and latent heat were computed using the usual expressions

$$Q_s = C_h \rho c_p \widetilde{(T_0 - T_a)} VA \text{ and } Q_e = C_e L \rho (q_0 - q_a) VA$$

where $\sim$ indicates areal averaging, V is the total wind speed, and A is area.

In addition to the foregoing, the Bowen ratio, r_b, was calculated using the relationship

$$r_b = \frac{Q_s}{Q_e} = \frac{c_p}{L} \frac{(T_0 - T_a)}{(q_0 - q_a)}.$$

A rough order of magnitude calculation was made of the infrared radiation from the top of an idealized inner cirrus shield. Using the equation $E = \sigma T^4$, where $\sigma = 8.22 \times 10^{11}$ cal. cm.$^{-2}$ min.$^{-1}$, the Stefan-Boltzman constant, assuming $T = 220$°A., which equates to an effective radiating cloud temperature of −53°C. located between the 150- and 180-mb. levels, one obtains the radiation in joules/day from an annular ring as

$$R_a = \frac{E\pi(b^2 - a^2)1440}{4.186},$$

where a and b are the pertinent radii.

The results of these calculations are presented in table 5, which shows that the air-sea temperature differences were close to 5.0°C. or about twice as large as those used by Miller [14] for hurricane Helene and by Riehl and Malkus [19] for hurricane Daisy. The air-sea humidity differences were also about twice those used by these investigators. Because of these similar proportions, the Bowen ratio was also quite similar, and varied from 0.15 to 0.21. Thus the latent heat added from the ocean surface was about five times the sensible heat given up by the water.

The bottom line of table 5 suggests that long wave radiation under the high cirrus shield was a minor factor at the inner radii, but one cannot conclude from this that radiation effects in hurricanes are unimportant. In a very interesting paper, Anthes and Johnson [1] recently computed the infrared radiation from the area outside the cirrus shield (from 500 to 1000 km.), using radiation rates from the Tropics as measured by Kuhn and Johnson [11]. Anthes and Johnson found that in hurricane Hilda on the same day, Oct. 1, 1956, the radiant loss of energy in the outer ring was equivalent to a cooling of the air mass at 1.5°C./day. This cooling in turn helped to contribute to the baroclinicity and to the production of available potential energy in quantities that were not insignificant when compared with that engendered by the release of latent heat at shorter radii. The effect of the increased albedo of the cloud shield in diminishing these baroclinic tendencies has apparently not been considered.

The budget for the total effective energy,

$$H = c_p T + gz + Lq$$

including the fluxes of sensible and latent heat, is shown

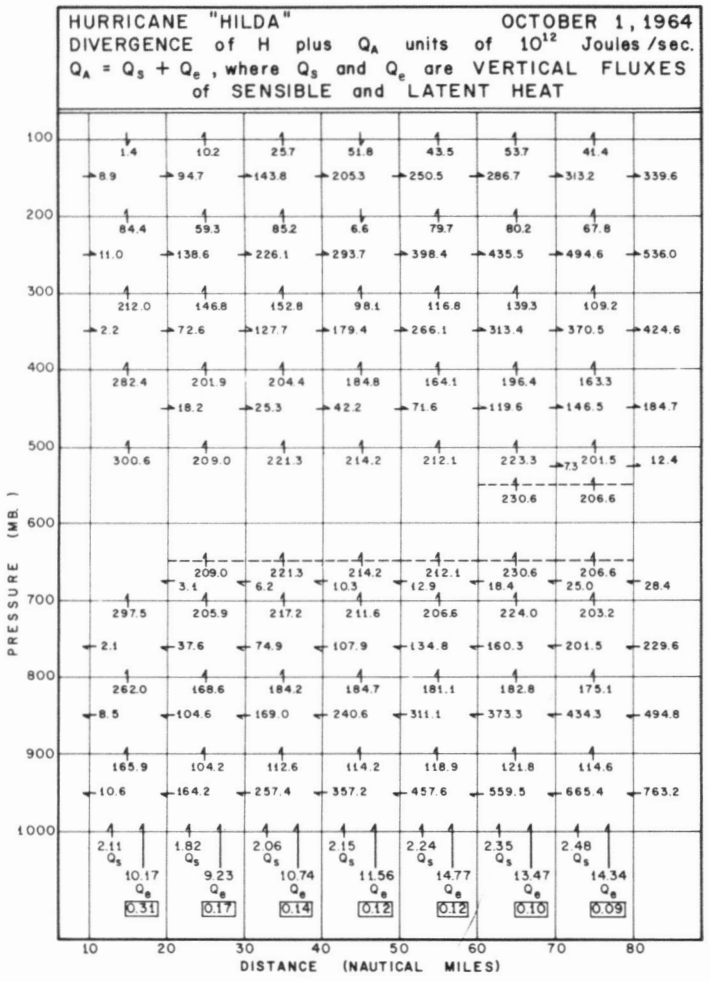

FIGURE 19.—Budget of $H = c_pT + Lq + gz$, the total effective energy, including the flux of sensible and latent heat from the ocean. Lowest numbers (enclosed) are the latent heat losses per unit area and time in units of joules cm.$^{-2}$ sec.$^{-1}$

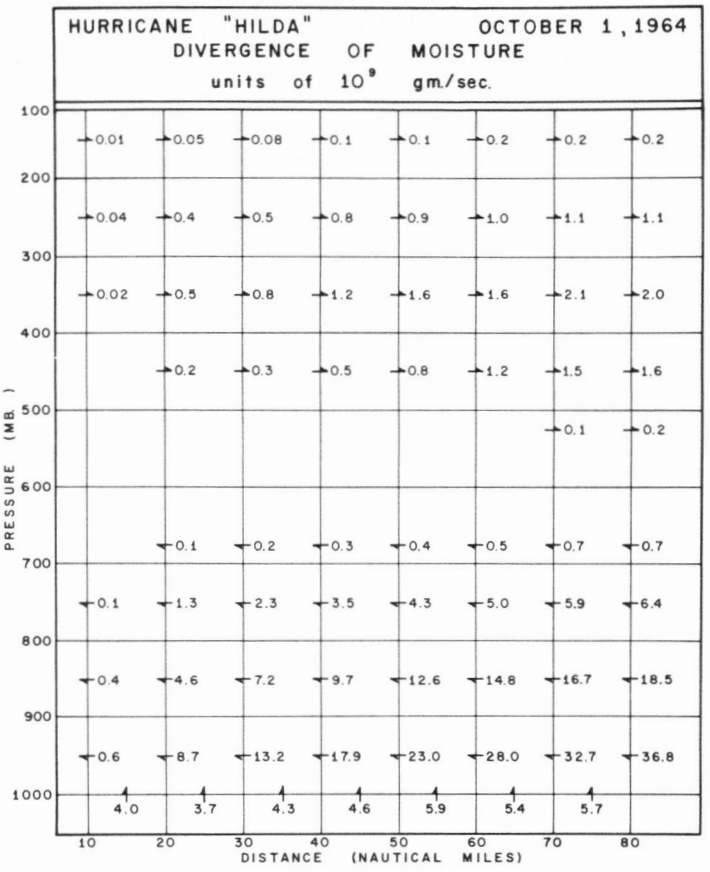

FIGURE 20.—Budget of moisture showing the horizontal mean transport and evaporation from the ocean surface.

TABLE 6.—*Rainfall rates for indicated annular rings assuming that all the convergent water vapor falls as precipitation*

HURRICANE "HILDA" OCTOBER 1, 1964
MOISTURE BUDGET AND RAINFALL RATES

RADIAL INTERVAL (N.Mi.)	10–20	20–30	30–40	40–50	50–60	60–70	70–80	10–80
DIVERGENCE q ($\times 10^9$ gm./sec.)	-16.9	-11.4	-11.9	-12.7	-13.3	-12.1	-12.0	-90.3
RAINFALL (INCHES/DAY)	17.7	7.1	5.4	4.5	3.8	2.9	2.5	4.5
TOTAL RAINFALL DURING PASSAGE OF INDICATED ANNULAR RINGS (INCHES) (6 Kt.)	2.43	0.98	0.74	0.62	0.52	0.40	0.34	6.0

in figure 19. Mean horizontal fluxes of H were computed from the rv_r curves using mean temperatures, mixing ratios, and heights for the appropriate pressure intervals. At the top of the diagram, a net excess/deficit for each annulus is indicated by an upward/downward arrow. An upward arrow indicates that energy in the amount cited was available for loss through radiative processes. Five of the rings show excesses but the amounts are of too large an order of magnitude to be accounted for by the expected radiative cooling at these radii. It seems more likely that the net annular amounts simply reveal limitations in data and procedures. At the one radial distance (about 50 n.mi.) at which the 900-mb. circumnavigation was made, a computation of the net eddy transport revealed that the transport was inward (in the same direction as the mean) but was only about 1 percent of the mean in magnitude.

The bottom row in figure 19 shows that the flux of latent heat from the sea surface diminished from 14.3 units in the outermost ring to 10.2 units in the innermost, or by a factor of ⅓, and that the flux per unit area of sea surface went from 0.09 units to 0.31 units over the same interval. Thus, over the innermost ring, despite the lower air-sea humidity difference, the ocean gave up to the atmosphere about three times as much latent heat per unit area as at the outer limits. The most efficient area in which to inhibit this transfer would be in the innermost rings where, however, the winds are strongest and the seas are the roughest. These latter factors have argued against experiments using monomolecular films to inhibit the transfer of water vapor and thus try to diminish the energy available to the storm. On the other hand, over the much larger area of the outermost ring, more total latent heat was supplied the storm under much less turbulent conditions, and under such conditions a

film would have a much better chance of remaining intact and effective.

8. BUDGET OF MOISTURE AND RAINFALL

Figure 20 presents the water vapor budget in units of 10^9 gm./sec. For comparative purposes one can convert these into joules/sec. ($\times 10^{12}$) used in figure 19, by multiplying the entries in figure 20 by 2.5. In the layer from 900 to 1000 mb., about 12 to 13 percent of the total effective energy was in the form of latent heat. In the layer from 800 to 900 mb., the latent heat represented about 10 percent of the total effective energy, while in the layer from 700 to 800 mb. it represented 7 to 8 percent of the total. Note that at the 50-n.mi. radius at 900 mb. (i.e., from 850 to 950 mb.) the eddy transport of water vapor was about 10 percent of the mean and in the same direction.

In table 6 the net convergence of water vapor in the annular volumes is indicated, together with the rainfall that might be expected if the "excess" vapor were condensed out. We see that the rainfall rate increased rather slowly with decreasing radius until the last two rings are reached, where the precipitation rate increased most abruptly. The lower line of the table gives the total rainfall that could be expected with the passage of the storm directly overhead, moving at its observed speed of 6 kt. The values include rainfall for both sides of the given annular ring. A total fall of 6.0 in. would be expected to occur during the passage of this inner portion of the storm (i.e., inner 80 n.mi.). Precipitation would also be expected outside this inner area so that the final total would probably fall in the range of 8 to 10 in. Since an average hurricane is "normally" expected to produce about 10 in. in passing, this total is not at odds with the usually accepted averages. Riehl and Malkus [19] calculated some 12 in. of precipitation for the passage of the inner 100 n.mi. of hurricane Daisy 1958 (on the 27th) and Miller [14] calculated some 7.3 in. for the passage of the inner 60 n.mi. of hurricane Helene.

9. BUDGET OF KINETIC ENERGY

An expression for the rate of change of kinetic energy in an annular volume may be derived from the horizontal equation of motion

$$\frac{d\mathbf{V}}{dt}=-f\mathbf{k}\times\mathbf{V}-\nabla\phi+\mathbf{F}$$

by taking the dot product with $\mathbf{V}$, assuming circular symmetry and setting $K=\frac{V^2}{2}$, the kinetic energy per unit mass.

$$\frac{\partial k}{\partial t}=-v_r\frac{\partial k}{\partial r}-\omega\frac{\partial k}{\partial p}-\mathbf{V}\cdot\nabla\phi+\mathbf{V}\cdot\mathbf{F}.$$

If we introduce the equation of continuity in its appropriate form

$$\left(\frac{\partial v_r}{\partial r}+\frac{v_r}{r}+\frac{\partial \omega}{\partial p}\right)=0,$$

and integrate over the mass of air in the annular volume (between 1000 and 100 mb.), we obtain

$$\int\frac{\partial k}{\partial t}\,dM=-2\pi\left[\iint\frac{\partial(rv_rk)}{\partial r}\,dr\,\frac{dp}{g}+\iint rv_r\frac{\partial\phi}{\partial r}\,dr\,\frac{dp}{g}-\iint\mathbf{V}\cdot\mathbf{F}\,rdr\,\frac{dp}{g}\right]$$

or,

$$\frac{\partial k}{\partial t}\,dM=-2\pi\int_{p_H}^{p_0}(v_{r_b}bk_b-v_{r_a}ak_a)\,\frac{dp}{g}-\pi(b^2-a^2)\int_{p_H}^{p_0}v_r\overline{\frac{\partial\phi}{\partial r}}^{a\text{—}b}\frac{dp}{g}+2\pi\iint\mathbf{V}\cdot\mathbf{F}\,rdr\,\frac{dp}{g}.$$

The first term on the right is the differential horizontal advection across radii a and b integrated over the vertical "limits" of the storm. It was evaluated over 100-mb. intervals from 1000 to 100 mb. The second term is the production of kinetic energy by pressure forces as the air parcels move across the isobars where the bar term is the mean from radius a to radius b. The third term, where $\mathbf{F}$ is friction, represents loss of kinetic energy due to frictional effects.

The results of these computations are presented in table 7, which shows that mean advection decreased steadily inward with decreasing radius. (Eddy transport across the 50-n.mi. radius at 900 mb. was slightly more than 10 percent of the mean advection and in the same direction, namely inwards.) The production of kinetic energy, on the other hand, increased with decreasing radius, reaching its maximum in the innermost annular ring. Overall, production contributed less that did advection to the increase of kinetic energy within the radii studied here. This is in contrast to the relative importance of these terms as determined by Riehl and Malkus [19] and by Miller [14].

The dissipation of kinetic energy due to friction can be subdivided into 1) losses caused by surface or ground friction and 2) losses resulting from internal friction. The

TABLE 7.—*Kinetic energy budget for the mean motion in hurricane Hilda*

HURRICANE "HILDA" KINETIC ENERGY BUDGET						OCTOBER 1, 1964 units of 10^{14} Kj./day		
RADIAL INTERVAL (N.Mi.)	10-20	20-30	30-40	40-50	50-60	60-70	70-80	10-80
MEAN ADVECTION	0.20	0.35	0.46	0.54	0.59	0.61	0.62	3.37
MEAN PRODUCTION	0.62	0.51	0.40	0.30	0.14	0.04	0.01	2.02
ADVECTION PLUS PRODUCTION	0.82	0.86	0.86	0.84	0.73	0.65	0.63	5.39
DISSIPATION DUE TO SURFACE FRICTION	0.76	0.67	0.59	0.51	0.42	0.36	0.32	3.63
LEFT OVER FOR INTERNAL FRICTION	0.06	0.19	0.27	0.33	0.31	0.29	0.31	1.76
RATIO OF INTERNAL FRICTION TO GROUND DISSIPATION	0.08	0.28	0.46	0.65	0.74	0.81	0.97	0.48

first may be approximated by the expression

$$F_0 = \int_A C_d \rho V^3 dA$$

which means that any estimate of internal friction must be determined through the use of residuals. Although this method leaves much to be desired, table 7 indicates that, despite the decreasing ground area of the smaller annular rings, surface frictional losses of kinetic energy increased as the radius decreased. This is not too surprising when one considers that the losses are proportional to the cube of the wind speed, which increases at smaller radii. However, the amounts left over for internal friction appear to be inadequate, particularly at smaller radii, a fact best reflected in the ratio of internal friction to that dissipated at the ground. It seems unlikely, though not impossible, that this rate should decrease as the radius decreases, i.e., as the winds and turbulence increase. In contrast to the investigators cited above, who found this ratio to increase with decreasing radius, we found by experiment that by doubling the production of kinetic energy in each annulus the ratio of internal to ground friction is maintained just about constant. We therefore concluded that while our budget may be deficient in certain respects it is probably correct to better than just the order of magnitude.

10. SUMMARY

The horizontal and vertical structures of the inner core of hurricane Hilda were examined in the detail permitted by the flights of Oct. 1, 1964. Greater vertical resolution and data from higher altitudes have permitted more detailed analyses and higher vertical coverage than previous data collections. Various budgets were prepared, which for the first time were drawn exclusively from aircraft data. The budgets compare rather favorably with those of previous investigators, who used a combination of conventional and aircraft data, but must be accepted with some reservations. Perhaps the major point with regard to the budgets is that they appear to be almost but not quite definitive. They suggest that for a storm offering better radar definition and hence more accurate compositing of the data, a similar collection of data would permit more definitive conclusions to be reached.

REFERENCES

1. R. A. Anthes and D. R. Johnson, "Generation of Available Potential Energy in Hurricane Hilda (1964)," *Monthly Weather Review*, Vol. 96, No. 5, May 1968, pp. 291–302.
2. H. R. Byers, *General Meteorology*, McGraw-Hill Book Co., Inc., New York, 1944, pp. 578–581.
3. E. L. Deacon and E. K. Webb, "Interchange of Properties Between Sea and Air," *The Sea*, Interscience Publishers, New York, Vol. 1, 1962, pp. 43–87.
4. W. M. Gray, "The Mutual Variation of Wind, Shear, and Baroclinicity in the Cumulus Convective Atmosphere of the Hurricane," *Monthly Weather Review*, Vol. 95, No. 2, Feb. 1967, pp. 55–73.
5. H. F. Hawkins, "Vertical Wind Profiles in Hurricanes," *National Hurricane Research Project Report* No. 55, U.S. Weather Bureau, Washington, D.C., June 1962, 16 pp.
6. H. F. Hawkins and D. T. Rubsam, "Hurricane Hilda, 1964: I. Genesis, as Revealed by Satellite Photographs, Conventional and Aircraft Data," *Monthly Weather Review*, Vol. 96, No. 7, July 1968, pp. 428–452.
7. L. A. Hughes, "On the Low-Level Wind Structure of Tropical Storms," *Journal of Meteorology*, Vol. 9, No. 6, Dec. 1952, pp. 422–428.
8. C. L. Jordan, "Mean Soundings for the West Indies Area," *Journal of Meteorology*, Vol. 15, No. 1, Feb. 1958, pp. 91–97.
9. E. S. Jordan, "An Observational Study of the Upper Wind-Circulation Around Tropical Storms," *Journal of Meteorology*, Vol. 9, No. 5, Oct. 1952, pp. 340–346.
10. P. Koteswaram, "On the Structure of Hurricanes in the Upper Troposphere and Lower Stratosphere," *Monthly Weather Review*, Vol. 95, No. 8, Aug. 1967, pp. 541–564.
11. P. M. Kuhn and D. R. Johnson, "Improved Radiometersonde Observations of Atmospheric Infrared Irradiance," *Journal of Geophysical Research*, Vol. 71, No. 2, Jan. 1966, pp. 367–373.
12. N. E. LaSeur and H. F. Hawkins, "An Analysis of Hurricane Cleo (1958) Based on Data From Reasearch Reconnaissance Aircraft," *Monthly Weather Review*, Vol. 91, No. 10–12, Oct.–Dec. 1963, pp. 694–709.
13. D. F. Leipper, "Observed Ocean Conditions and Hurricane Hilda, 1964," *Journal of the Atmospheric Sciences*, Vol. 24, No. 2, Mar. 1967, pp. 182–196.
14. B. I. Miller, "On the Momentum and Energy Balance of Hurricane Helene (1958)," *National Hurricane Research Project Report* No. 53, U.S. Weather Bureau, Washington, D.C., Apr. 1962, 19 pp.
15. B. I. Miller, "A Study of the Filling of Hurricane Donna (1960) Over Land," *Monthly Weather Review*, Vol. 92, No. 9, Sept. 1964, pp. 389–406.
16. B. I. Miller, "Energy Exchanges Between the Atmosphere and the Oceans," *American Society for Oceanography Publication No. 1, Hurricane Symposium, October 10–11, 1966, Houston, Texas*, pp. 134–157.
17. J. J. O'Brien and R. O. Reid, "The Non-Linear Response of a Two Layer, Baroclinic Ocean to a Stationary, Axially Symmetric Hurricane: Part I. Upwelling Induced by Momentum Transfer," *Journal of the Atmospheric Sciences*, Vol. 24, No. 2, Mar. 1967, pp. 197–207.
18. E. H. Palmén and H. Riehl, "Budget of Angular Momentum and Energy in Tropical Cyclones," *Journal of Meteorology*, Vol. 14, No. 2, Apr. 1957, pp. 150–159.
19. H. Riehl and J. Malkus, "Some Aspects of Hurricane Daisy, 1958," *Tellus*, Vol. 13, No. 2, May 1961, pp. 181–213.
20. S. L. Rosenthal, "Concerning the Mechanics and Thermodynamics of the Inflow Layer of the Mature Hurricane, *National Research Project Report* No. 47, U.S. Weather Bureau, Washington, D.C., Sept. 1961, 31 pp.
21. J. R. Stear, "Sounding in the Eye of Hurricane Arlene to 108,760 Feet," *Monthly Weather Review*, Vol. 93, No. 6, June 1965, pp. 380–382.

[*Received December 12, 1967; revised March 27, 1968*]